MOTIONS AND STRUCTURE OF THE FILAMENTARY ENVELOPE OF THE CRAB NEBULA

Thesis by

Virginia Louise Trimble

In Partial Fulfillment of the Requirements

For the Degree of

Doctor of Philosophy

California Institute of Technology

Pasadena, California

1968

(Submitted April 17, 1968)

Dedication:

To that Bright Spirit

Who once said: "Come! Fly with me."

And gave me the Universe

To fly toward

PREFACE

The first four sections of the present dissertation comprise the manuscript of a paper prepared for submission to the Astronomical Journal. The last section includes both additional discussion of the data presented in the paper and new work on the distribution of energy and temperature in the nebula. As a result, some data appear in more than one place.

The four happy years I spent as a graduate student, as well as this dissertation, were made possible by the Woodrow Wilson Foundation, California Institute of Technology, and the National Science Foundation, who supported me in a style to which I never quite became accustomed.

There do not seem to be any words adequate to express my gratitude to Dr. Guido Münch. He originally suggested this project and has patiently re-aimed me whenever I went astray. For his kindness, encouragement, and knowledge freely shared, I can only say "thank you."

My sincerest thanks are also due to Drs. Jesse L. Greenstein, Jan H. Oort, Richard P. Feynman, and James E. Gunn who read the manuscript in various states of completion and made many helpful suggestions, and to Dr. Greenstein additionally for my first chance at authorship,

To Drs. Rudolph Minkowski and Peter Scheuer for several illuminating conversations, and to Dr. Minkowski also for permission to use spectra taken by him,

To my fellow students, especially Bruce and Vicki Peterson, Doug Keeley, and Drs. Jeffrey D. Scargle and Christopher M. Anderson, for listening patiently to numerous one-sided conversations on the virtues of the Crab Nebula,

To Dr. Albert Wilson for introducing me to the mysteries of the 48 in. Schmidt telescope,

To Dr. Harold Zirin for efforts above and beyond the call of duty in nursing me through the oral qualifying examination,

To Dr. J. Beverley Oke for much valuable advice on how to become, remain, and cease to be a graduate student,

To Susan Kayser, Vicki Peterson, Donna Weistrop, Sue Werner Kieffer, and Judy Cohen, my office mates in the "nunnery," for their patience with my strange and untidy work habits,

To Henrietta Swope and Louise Lowen for locating plates in the Mt. Wilson Observatory files and entrusting me with them,

To Drs. Maarten Schmidt, Kip Thorne, Charles Bures, and William Fowler whose lectures were a particular joy,

And most of all to my parents for their constant love and their willing acceptance of their daughter's curious pursuits.

TABLE OF CONTENTS

ABSTRACT

Proper motions have been measured for 132 line-emitting filaments in the Crab Nebula on direct plates taken with the 100 and 200-inch telescopes. These motions, if assumed constant and extrapolated backwards in time, converge toward a point about 12" southeast of the double star near the center of the nebula. The filaments approach, on the average, most closely to that point or expansion center in about the year 1140, indicating that the expansion has been somewhat accelerated.

Proper motions and radial velocities were measured for an additional 126 features on the same direct plates and Mt. Wilson and Palomar spectra. These, along with other, nondynamical data, indicate a most probable distance to the object of 2.02 kpc. Two projections of the nebula perpendicular to the one seen in the plane of the sky are constructed and do not differ significantly from that presented to us.

The proper motion and radial velocity of the nebula as a whole are found and converted into galactic coordinates. This requires several assumptions of questionable validity. The nebula seems to be moving about 112 km/sec faster than the galactic rotation at its position. The proper motion of the so-called central star translates into an equally unlikely space motion, but this is also extremely uncertain. The likelihood of a physical connection between the star and the nebula is discussed.

The line-emitting filaments are shown to be distributed

throughout the nebula rather than being confined to a thin outer envelope. The motions are largely radial, each filament having a velocity approximately proportional to its distance from the expansion center. The deviations from this proportionality are as large as .032"/yr or 300 km/sec and have mean values near .010"/yr or 70 km/sec. These deviations are correlated with the scatter of the filaments around the expansion center in 1140.

Photographic materials on pp. 99 and 101 are essential and will not reproduce clearly on Xerox copies. Photographic copies should be ordered.

I. INTRODUCTION

The Crab Nebula now occupies that part of the sky where the Chinese reported seeing a "guest star" or supernova in 1054 (Duyvendak, 1942). It is the only historically well documented supernova remnant readily accessible to study by optical methods. Despite its uniqueness and availability, its internal motions and structure have by no means been completely described. The present paper attempts such a description based upon newly obtained proper motions and radial velocities of that component of the nebula characterized by a filamentary structure and a line emission spectrum. The nebula also emits continuous radiation which is relatively featureless.

The filaments define quite accurately an ellipse in the plane of the sky, except for a bulge on the south preceeding edge. The ellipse has its center about 4".7 east of the north following component of the 15th magnitude double star near the center of the nebula (Baade, 1942). The axes of the ellipse are about four and six minutes of arc in length, the major axis lying in position angle $133^{\circ}28'$.

The best proper motions previously published (Duncan, 1939), representing just twenty features near the edges of the nebula, clearly reveal a radial expansion. These motions have been analyzed (Duncan, 1939; Baade, 1942; Brosche, 1966) to determine the center of that expansion and its time scale. The distance to the object has also been derived from these motions and radial velocities. Considerable improvement in quantity and quality of proper motions and the resulting analysis is now possible.

Woltjer (1958) and Münch (1958) have published radial velocities for more than one hundred positions in the nebula. These positions were not indicated with sufficient accuracy that a given velocity could be identified with any particular feature on a direct plate. Such identifications can now be made.

II. MATERIALS AND MEASURING TECHNIQUES

Six direct plates, as listed in Table I, all taken in the light of the H_α and [NII] emission lines, were measured for proper motions.

TABLE I

DIRECT PLATES USED IN PROPER MOTION STUDY

Date	Telescope	Plate	Filter	Exposure	Observer	Filaments Measured
1939	100 in.	*	RG2	178 min	Baade	1 - 259
1953	"	103a-E	RG2	165	Baade	1 - 259
1966	"	Ia-E	RG2	120	Münch	132 - 259
1950	200 in.	103a-E	RG2	45	Baade	1 - 259
1964	"	103a-E	RG1	67	Münch	1 - 259
1966	"	103a-E	H_α	70	Münch	132 - 259

*Ammoniated red-sensitive plate, approximately equivalent to modern 103a-E.

These plates have two advantages over the earlier 60" plates used by Duncan. First, of course, the larger scale (16.00 "/mm on the 100 in. and 11.14 "/mm on the 200 in. plates) allows positions to be determined more accurately. Secondly, the isolation of these emission lines by the use of a color filter and red-sensitive plates reveals a vast number of sharp, discrete features or filaments (Fig. 1). The earlier orthochromatic plates, taken without any filter, show primarily the featureless continuum emission. Only a

few of the strongest filaments appear in the light of H_β and N1 and N2.

The filaments first measured for proper motion (No. 1-132 of Table III and Fig. 1) are more or less uniformly distributed over the surface of the nebula. They are all small, distinct, and readily identifiable on all six plates.

Each of the four earliest plates was measured in four orientations differing by 90°. Settings were made with cross-hairs on the ground glass projection screen of a Grant measuring machine (described in Greenstein and Trimble, 1967). The 200 in. plates were also measured with a conventional traveling microscope. The plates were oriented by aligning two stars (A and B of Fig. 1) on the cross-hairs. Positions of 132 filaments and 35 reference stars were recorded with respect to the axis through these stars (Position angle $76^\circ 18'$) and later rotated to right ascension and declination coordinates.

The measured positions were reduced using the method of dependences (van de Kamp, 1962). This was done twice. Each filament was compared first with the four stars closest to it and then with all the stars (except the south preceding component of the central double star, E in Fig. 1, which has considerable proper motion). The results from the two measuring engines and the two methods of reduction do not differ by more than the inaccuracy of a single setting (2 to 5 microns, depending on the size and shape of the feature involved). Quite by chance, the scales and time separa-

tions of the plates are such that a one micron difference in position between the 1939 and 1953 or the 1950 and 1964 plates corresponds to about .001"/yr of proper motion. The tabulated values are those obtained from the Grant machine and the reduction using all the stars.

Twenty-four spectra from the Mt. Wilson and Palomar Observatories plate collection were measured for radial velocities. The eighteen spectra taken by Münch include those previously published (Münch, 1958). Most of these were taken with the nebular spectrographs of the 100 in. and 200 in. telescopes. The 300 groove/mm grating used is blazed in the IIIrd order at H_α and gives dispersions of 110 Å/mm or 215 Å/mm, depending on the focal length of the camera. A few other plates, taken with a different grating, have dispersions near 400 Å/mm. Table II lists the lines measured.

TABLE II

EMISSION LINES MEASURED IN SPECTRA OF CRAB NEBULA

Wavelength	Element	Intensity
6730.48	[SII]	Medium
6716.42	[SII]	Medium
6583.37	[NII]	Strong
6562.82	H	Strong
6548.06	[NII]	Strong
6300.27	[OI]	Faint, often absent

Six plates at 215 Å/mm taken by Minkowski were also measured. These have the third, fourth, and fifth orders overlapped (but only a third order comparison spectrum) and, therefore, show many more lines. Only [NII] and H_α were measured.

All spectra were measured using the oscilloscope of the Grant measuring machine. A single spectrum (Fig. 2) shows from three to thirty separate features. The streaks perpendicular to the slit directions are stars. Two or more features overlap in many cases (for example, point X in Fig. 2). This overlapping reduces the accuracy with which the positions of the lines can be determined. Fortunately the spacing of the emission lines is such that if the [SII] lines of two features are blended, the [NII] and H_α lines are not, and vice versa. Where there is no blending, settings on the Grant machine are usually repeatable to within one micron (5 to 20 km/sec at the dispersions involved). The standard deviations of velocities determined from several lines are generally in this range.

Curvature of the spectral lines perpendicular to the direction of dispersion is the other main source of error. The apparent difference in velocity between two positions along the slit due to this curvature can easily be calculated for a perfect optical system (Minkowski, 1942a). It should depend only on the distances of the two positions from the center of the slit and on the focal length of the camera.

As a check on the calculated values, empirical curvature corrections were determined from several calibration plates having

comparison lines along the full length of the slit. These plates were taken at the same time and with the same optical set-ups as the various spectra. Pairs of such plates taken with the same camera and grating on the same telescope were not entirely in agreement, and the curvature correction was found to be a function of wavelength. This may reflect a dependence on distance from the optical axis of the system. On the widest 200 inch telescope spectra, for example, the calculated velocity shift between the center of the spectrum and the point where the comparison lines were measured was 103 km/sec. The observed shift on one calibration plate ranged from 71 km/sec at the [SII] lines to 114 km/sec at the [OI] line, while another plate taken the same year with the same optical set-up showed a range of 77 to 154 km/sec over the same wavelength region.

The velocities from each spectrum of the nebula were corrected in accordance with the calibration plate taken with the same camera and grating at most nearly the same time. The resulting error may be as great as 15 km/sec for the velocities of a few filaments furtherest from the comparison lines. In most cases, it is less than 10 km/sec.

About 25 features appear on two or more (parallel or intersecting) spectra. Where this occurs, the several velocities for a single filament differ by less than their probable errors. The velocity tabulated for such a filament is the average of the values from the various plates.

Positions of the features along the slit (with respect to stars

on plates where they occur, otherwise with respect to the center of the slit) were recorded at the time the spectra were measured. Using these positions, the spectra were compared with direct plates. Because Münch's original observing charts were still available, velocities could be associated with particular features on the direct plates for all but two of the spectra. It became possible to do this for Minkowski's spectra only after the proper motion measurements had been completed.

The 127 features with known radial velocities found in this way (No. 133 - 259 of Table IV and Fig. 3) were then measured with the Grant machine on all six direct plates. These were reduced in the same fashion as the first set of proper motion measurements for the five pairs of plates 1939-53, 1939-66, 1953-66 (100 in.) and 1950-64 and 1950-66 (200 in.). A proper motion in Table IV is the mean of the resulting five numbers. Since these features could not be chosen for ease of measurement on the direct plates, a single setting may be in error by 4 to 8 microns. These filaments are also much less uniformly distributed over the nebula than was the first set of features.

III. RESULTS

A. Proper Motions

Figure 1 shows the first set of filaments for which proper motions were determined. Many of the fainter features have been lost in the reproduction process, but they are easily seen and measured on the original plates. The arrows show the distance each filament will cover in about 270 years at its present rate of motion. Table III lists the coordinates, x and y, (for 1950) and proper motions, μ_x and μ_y, of the filaments identified in Figure 1. Following Duncan (1939), these are given in seconds of arc in a rectangular coordinate system which corresponds to right ascension and declination near the center of the nebula. The origin is the north following component of the central double star (D in Fig. 1). The tabulated proper motions are the averages of the results from the two pairs of plates. These motions and all those tabulated and discussed below are relative to the group of 35 reference stars. The motions found for these stars are given in an appendix.

The table also gives the total proper motion vector, μ_r, and its position angle, α, for each filament. The percentage error of the length, E_μ, is one half the difference of the 100 in. and 200 in. results expressed as a per cent of their average. This is less than 4.5% for one half of the filaments and less than 11% for three quarters of them. The probable error of the angle, σ_α, is one half the difference of the 100 in. and 200 in. results. This is less than 3^o for one half of the filaments and less than 5^o for three quarters of them.

There is no systematic difference in the angles determined from the two sets of data, but the 200 in. motions are, on the average, 3% larger than the 100 in. ones.

The sets of data from the two pairs of plates were analyzed separately to determine the center of expansion and the time when the filaments were, on the average, closest to that center. This was done in two ways. In the first case, the center was taken to be a weighted mean of the 8,712 positions of the intersections of all possible pairs of proper motion vectors. The weight given to each point was the reciprocal of the distance that point is moved by a small change in one of the two motions involved. (This depends both on the lengths of the vectors and on the size of the angle between them.) The time was then found when the filaments were closest to that center, if their velocities have been constant.

In the second case, the center was taken to be that point to which all the filaments approached most closely (in a least squares sense) at a single time. That time was also determined. It can be easily shown (by using, for example, three vectors which form a scalene triangle) that these two methods need not give the same answer.

Table V lists the results of these various operations. The coordinates again follow Duncan's convention. The positions found for the center are shown as C1, C2, C3, and C4 in Fig. 4 along with the five stars near the center of the nebula (C through G of Fig. 1). All of the centers (which are located about 12 arcsec southeast of the

north following star, D) fall within less than 6" of one another.

TABLE V

EXPANSION CENTERS AND DATES OF CONVERGENCE OF CRAB NEBULA

Center	Plates	Reduction Method	Right Ascension of Center	Declination of Center	Date of Best Convergence
C1	100 in.	Weighted Mean	+6".3	-10".3	1131
C2	100 in.	Least Squares	+5".6	- 8".7	1134
C3	200 in.	Weighted Mean	+9".1	- 8".7	1147
C4	200 in.	Least Squares	+9".4	- 6".3	1149
	Average		7".6±1".3	-8".5±1".1	

The convergence of the filaments at the dates indicated is quite good. One half of the filaments fall within a circle of radius 6".4 around the center according to the 200 in. data. The corresponding area for the 100 in. data is an ellipse 8.1 × 9".5. These areas are shown in Fig. 4.

The date of best convergence is about 1140AD -- that is, somewhat earlier than Duncan found, but still far from 1054. The sixteen year difference between the two sets of data indicates that the error of the measurements is probably much less than this 90 or so years. Since convergence occurs later than 1054, evidently the present proper motions are larger than the average proper motions over the lifetime of the nebula. This could be accounted for by a gradual uniform acceleration. More or less random or pulsation-

like variations about some mean velocity of expansion are also possible. If the sixteen year difference between the 100 in. and 200 in. results is real, it would tend to indicate a gradual acceleration, since the more recent pair of plates shows the larger velocities. Comparison of any of the dates with Duncan's results (1172AD, found from a 1909-1938 baseline) indicates quite the opposite. The 3% apparent increase in average motion mentioned above is, in any case, much too large to be interpreted as part of an approximately uniform acceleration since it occurs in only eleven years.

Convergence dates were also found for the filaments lying near the major and minor axes of the nebula separately. These do not differ to within the accuracy of the determination (25 or so years, since fewer filaments are involved). This negative result indicates only that the nebula has expanded out of a very small area, as has already been shown. If the dates had differed systematically, in the sense of the major axis date being earlier than the minor axis date it would have indicated either that the velocity field was established at a time when the nebula was already reasonably large and elliptical in shape or that the rate of acceleration along the minor axis has been smaller than along the major axis. A later major axis date would have indicated greater acceleration along the minor axis direction.

The proper motion of the nebula as a whole ought to be given by (present position of the center of mass - position of expansion center) ÷ age. The geometrical center of the ellipse (in the plane of the sky) filled by the faintest filaments is easily found. It is (Baade, 1942) 4".7 ± 3" east and 0".0 ± 3" north of the north following star.

There is, however, no particular reason to suppose that this coincides with the center of mass. Indeed, the concentration of both bright filaments and the brightest continuum emission on one side of the geometrical center indicates strongly that they do not coincide. In addition, both the radio emission at various frequencies and the X-ray emission from the nebula appear to have their centers northwest of the optical center (Matveenko and Sorochenko, 1968; Bowyer et al., 1964; Oda et al., 1967). The small, low-frequency radio source, on the other hand, is about 10" southwest of the optical center (Gower, 1967). Most of the activity observed in the continuum emission (discussed by Scargle, 1968) is also on the northwest side of the geometrical center. Although some of that activity takes the form of outward moving, slightly curved wisps, their center is not sufficiently well determined to differentiate between the various other centers.

In addition, the assumption that the mass and geometrical centers are coincident yields an extremely unlikely value for the space motion of the nebula. This point will be considered again after a discussion of the distance to the Crab Nebula, since this distance determines just how unlikely the resulting space motion will be.

Any attempt to find the overall proper motion by analysis of the motions of individual filaments is also frustrated by this uncertainty of the center of mass coordinates.

Six of the stars measured have detectable proper motion (see Appendix). One of these is the south preceeding component of the central double star. Previously published values for its motion are

seriously discordant. Duncan (1939) and Deutsch and Lavdovsky (1940) find μ_α = -.019"/yr and -.018"/yr respectively and μ_δ very nearly zero. Baade (1942) and van Maanen (1928) find μ_α = -.009"/yr and -.007"/yr respectively and confirm μ_δ near zero. The present measurements of all six direct plates give μ_α = -.009"/yr with a probable error of .003"/yr and μ_δ = -.002"/yr with a similar probable error. Fig. 4 shows the positions of the south preceding star in 1054, for both the larger and the smaller proper motion, as E1 and E2. This position is just the 1950 position minus $\mu \times$ (1950 - 1054). Baade, in calculating the position of this star at the time of the supernova explosion, made the curious assumption that the number of years entering into the sum should be (present date - 1172) as though the star's motion had participated in the apparent acceleration of the nebular expansion. This seems to be totally unwarranted.

Neither proper motions brings the star's 1054 position within the region where the expansion center of the nebula most probably lies, but the coincidence is much closer than with Duncan's expansion center, which, on the scale of Fig. 4, lies a bit off the left side of the page at about the height of star C. The positions found for the star and nebula are not quite so near as might be expected if they are the remains of a single event, but the close approach is nevertheless suggestive, particularly since none of the other stars near the center of the nebula has a detectable proper motion.

Although there are no known spectra of stars which are remnants of supernovae anywhere near as old as the Crab Nebula, it might

be expected that, if this star is physically connected with the nebula, it ought to be unusual in some way or other. Unfortunately it is not an easy star to observe because of the strong continuous emission of the surrounding nebula. Two spectra of the star have been taken at the Mt. Wilson and Palomar Observatories. The earlier one, taken by Minkowski (1942b), has no detectable lines. The more recent spectrum, taken by Kraft (1967), is somewhat underexposed, but appears to show weak lines of hydrogen and ionized calcium in absorption. Both of these spectra probably have a large and perhaps predominant component due to the nebular emission. If the star is, as the Kraft spectrum indicates, not very peculiar, then the probability of its being related to the nebula is greatly decreased. There are, after all, six stars very near the center of the nebula (C through G of Fig. 1 and a 21st magnitude star between E and F).

B. The Distance to the Crab Nebula

Before the proper motion and radial velocity data in Table IV can be combined to give a three-dimensional picture of the Crab Nebula, its distance must be known. The dynamical data themselves suggest a range of probable distances within which a choice must be made on the basis of other considerations.

If the nebula were a uniformly expanding sphere or spherical shell, then the distance, D, might be found by setting the maximum observed radial velocity, V_r^{max}, (which ought to occur at the center of the nebula) equal to the maximum observed proper motion, μ^{max},

(which should occur at the edges) in the formula,

$$V_r^{max} = 4.74\ \mu^{max} D \qquad (1)$$

where D is in parsecs, V_r^{max} in km/sec, and μ^{max} in arcsec/yr. Unfortunately, the object is, at best, some sort of an ellipsoid, and the blind use of formula (1) clearly implies the assumption that the axis of the ellipsoid along the line of sight is the same length as the major axis of the ellipse in the plane of the sky. An equally reasonable assumption might be that the axis along the line of sight is the same length as the minor axis in the plane of the sky. Anything in between or somewhat outside of this range is also, of course, possible. Distances have been calculated for only these two simple assumptions out of prejudice in favor of symmetry.

The largest measured radial velocities (filaments 220, 221, 246, and 247 of Table IV) seem, with some regard to their probable errors, to indicate a maximum of about 1450 km/sec. The largest velocities measured on Minkowski's plates, -1446 ± 18 km/sec and +1482 ± 41 km/sec, confirm this.

The largest proper motions along the major axis are all about .222"/yr (filaments 58, 59, 125, and 127 of Table III). The procedure used by Baade to correct Duncan's proper motions to what they might have been if the features measured had been at the extreme ends of the major axis is in this case both unnecessary (since the filaments are very nearly there already) and unwise (since it assumes an absolutely uniform expansion). Any number in the range .220 to .225"/yr

would be equally consistent with the data, but the value chosen has the particular virtue that .222"/yr × 810 years = 180", the length of the major axis.

Along the minor axis an unexpected difficulty arises. Some of the motions are much too large. Since the axial ratio of the ellipse in the plane of the sky is very nearly 2/3, the largest proper motions near the ends of the minor axis ought to be about 2/3 × .222"/yr or .148"/yr. There are, in fact, filaments (21, 22, 23, and 73 of Fig. 1 and Table III) fulfilling this expectation ($\bar{\mu}$ = .151"/yr). There are, however, other features near the minor axis having larger velocities. A couple of these (26 and 52) are located in the "bulge" which extends outside the otherwise well-defined ellipse on its south preceding edge. Their larger proper motion (about .163"/yr) is, therefore, not disturbing. Other filaments (33, 72, 121, and 122), however, lying near the minor axis but not in the bulge have proper motions near .171"/yr.

Filaments with motions smaller than the values listed also occur near the ends of both axes. These are of the order of .140"/yr near the end of the minor axis and .200"/yr for the major axis. Alternatively, therefore, the largest minor axis proper motions might have been taken as "normal" and the absence of major axis motions as large as .258"/yr (3/2 × .172"/yr) be regarded as surprising. Since the smaller motions have, at least, the virtue of actually occurring somewhere near the edges of the nebula, they will be used.

Returning to formula (1) and inserting V_r^{max} = 1450 km/sec and μ^{max} = .222 or .151"/yr reveal that the Crab Nebula can be either an oblate spheroid at a distance of 1.38 kpc or a prolate

spheroid at a distance of 2.02 kpc (or, in principle, any other consistent combination). The uncertainty of these numbers is rather great. If the largest and smallest possible values of proper motion and radial velocity indicated by the discussion above are put into formula (1), the distance for the oblate spheroid is found to range from 1.15 to 1.61 kpc and that of the prolate spheroid from 1.76 to 2.26 kpc.

The only other "distance" that can be found from the data of Table IV is the one that comes from assuming that all the filaments ought to have, as nearly as possible, the same total speed. This would be precisely true for a uniformly expanding thin spherical shell. Applying the assumption to the Crab Nebula gives a distance of 2.17 kpc, not very different from that just found for a prolate spheroid.

Because the positions of the filaments along the line of sight are not known, no estimate of the distance can be derived by requiring the filaments to come as close as possible to a single point (in three dimensions) at a single time, or from any similar consideration.

A number of independent, non-dynamical arguments favor a distance around 2 kpc. Woltjer (1958) points out that a quantity involving the line ratio $[\,OIII]_{N1+N2}/[\,OII\,]_{\lambda 3727}$, which ought to depend only on electron density, becomes nearly constant over the nebula only if this larger distance is assumed. If the smaller distance is correct, then the quantity depends strongly on the distance of an emitting filament from the center of the nebula.

Münch (1958) suggests that, since the direction of the major axis of the ellipse enclosing the filaments is very nearly the direction

of the galactic equator at that point in the sky, the shape of the nebula might have been influenced by the interstellar magnetic field, the matter expanding most rapidly along lines of force (assumed parallel to the galactic equator). Both the minor axis direction and the line of sight are perpendicular to these lines of force, and the axes in these directions ought to be roughly equal and smaller than the major axis.

Minkowski (1964) favors the larger distance as bringing the maximum brightness of the observed supernova (deduced from the Chinese records) closer to the average of Type I events in other galaxies. The frequency of supernovae in our galaxy is also more like that found for the Virgo cluster if the larger of two possible distances is assumed for the Crab Nebula as well as for Tycho's and Kepler's supernovae. If, as has recently been suggested, (Minkowski, 1966), the supernova of 1054 was not a Type I event, this argument ceases to be relevant. His only counterargument is the large mass of the filaments implied by the larger distance. Shklovskii (1966) points out that the prolate shape associated with the larger distance is in better agreement with what is known about the ejection of matter from novae and explosions in galactic nuclei than is the oblate shape implied by a distance around 1 kpc. In addition, the interstellar absorption expected out to 2 kpc or so is sufficient that the continuous emission from the nebula can then be interpreted as synchrotron radiation with a constant spectral index over the entire frequency range $10^{12} - 3 \times 10^{16}$ cps. If the smaller distance is assumed, the spectral index must vary with frequency. He also notes that the mass of the filaments

implied by the larger distance need not be intolerably large.

The two arguments dealing with the way in which the nebular matter was ejected tend also to favor the assumption of axial symmetry made above. The ensuing discussion will, therefore, suppose that the Crab Nebula is 2.02 kpc from us.

C. Three Dimensional Considerations

Table IV gives the positions, proper motions, and radial velocities of the 127 filaments identified in Figure 3.

The radial velocities of individual filaments reveal the same sort of non-uniformity that was noted in the case of the proper motions. Just as the proper motions do not reach a unique maximum value at the edge of the nebula, the radial velocities do not tend to zero there; nor are the largest velocities found precisely at the center of the nebula. It is, therefore, only approximately true that the velocity of each filament is proportional to its distance from the expansion center. The fact that all filaments do converge to such a center at a single time shows that there is, in general, such a proportionality.

The resulting uncertainty in positions of filaments along the line of sight can be estimated. Proper motions at the extreme ends of the minor axis in the plane of the sky vary from .140 to .172"/yr, a range of .032"/yr, and radial velocities as large as 300 km/sec are found very near the edges of the nebula. Formula (1) shows that, for a distance of 2020 pc, these two numbers represent very nearly the same space motions. A filament of known radial velocity will, there-

fore, have a 1950 position along the line of sight given by its velocity times the age of the nebula (2.5×10^{10} seconds), but that position will be uncertain by about 7×10^{12} km, or, in unreasonable units, 25 seconds of arc projected to a distance of 2020 parsecs. This is about the distance, in the plane of the sky, from star C to star G, or a bit more than one tenth of the minor axis. Subject to this limitation on accuracy, cross-sections of the nebula perpendicular to the one shown in Figure 3 can be constructed.

Figure 5 shows the positions and motions in 270 years of filaments 133-259 in the major axis - line of sight cross-section. Figure 6 represents the minor axis - line of sight cross-section similarly. The side of the nebula toward us is at the bottom of Fig. 5 and to the left in Fig. 6. Both these cross-sections appear rather circular. This is expected in the case of Fig. 6. In Fig. 5 it is a result of the total absence of filaments of known radial velocity anywhere near the ends of the major axis. The non-uniform distribution of the features over the nebula is also evident. When this non-uniformity is taken into account, these cross-sections do not appear to differ significantly from the one presented to us in the plane of the sky. In particular, the stronger connected features visible on a direct plate can be readily traced in all three cross-sections. It is interesting to note that the strongest of these are often the result of the superposition of two emitting regions on opposite sides (from our point of view) of the nebula.

If the assumption that the present geometrical center of the

nebula coincides with its center of mass is correct, then the object as a whole has a proper motion (given by present center position minus expansion center position divided by age) μ_α = -.0036"/yr and μ_δ = +.0105"/yr, or a total of .0111"/yr in position angle 341°4'. (This should be compared with the proper motion of the so-called central star, μ_α = -.009"/yr, μ_δ = -.002"/yr.) For a distance of 2020 pc, the motion of the nebula is equivalent to 102 km/sec.

Because the location of the geometric center is determined only within about 3" in each direction and the location of the expansion center to within about 1", all of these quantities are somewhat uncertain. This uncertainty amounts to .005"/yr for each component of the proper motion or more than 55 km/sec in the total motion and 40° in its orientation. Any discussion of the total space motion of the Crab Nebula must therefore be regarded with considerable skepticism.

An average radial velocity for the nebula can also be found if all the filaments are assumed to lie on the surface of a prolate spheroid located at a known distance. It must also be assumed that, in the reference frame of the nebula, each filament has its velocity proportional to its distance from the expansion center. As is pointed out above, this is only approximately true. Under these assumptions, the radial velocity of the nebula is that V_R which makes

$$\sum_i \left(V_{r_i} - V_R\right) = \frac{4.74\,b}{\pi} \sum_i \frac{\mu_{x_i}}{x_i} \left[1 - \left(\frac{x_i}{a}\right)^2 - \left(\frac{y_i}{b}\right)^2\right] \qquad (2)$$

and

$$\sum_i \left(V_{r_i} - V_R\right) = \frac{4.74\,b}{\pi} \sum_i \frac{\mu_{y_i}}{y_i} \left[1 - \left(\frac{x_i}{a}\right)^2 - \left(\frac{y_i}{b}\right)^2\right] \qquad (3)$$

where the sum is taken over all the filaments; x and y are coordinates of a filament in arcsec along the major and minor axes of the ellipse in the plane of the sky; a and b are the semi-axes of that ellipse, 178" and 120" respectively; μ_x and μ_y are proper motions in arcsec/yr along these axes; π is the assumped parallax (1/2020); and V_r is the radial velocity of a filament in km/sec. The velocity found by this method is -5.5 km/sec, confirming earlier statements (Baade, Woltjer) that the motion of the object is very nearly all in the plane of the sky.

The motion of the nebula with respect to the galactic plane and the local standard of rest is then easily found by transforming to galactic coordinates ($\ell = 184^o$, $b = -6^o$) and subtracting the basic solar motion ($\Pi = -9$ km/sec inward toward the galactic center; $\Theta = 11$ km/sec faster than the circular velocity at the sun's position; and $Z = 6$ km/sec upward from the plane of the galaxy. Delhaye, 1965). The resulting velocities are $\Pi = -11$ km/sec, $\Theta = +114$ km/sec, and $Z = +33$ km/sec.

A population I object following a nearly circular orbit at the position of the Crab Nebula would have Π and Z near zero and Θ about -12 km/sec. This is just the difference of the circular velocities at the position of the sun (250 km/sec) and the nebula (238 km/sec; Schmidt, 1965). A population II object lagging behind the galactic rotation would have Θ still more negative. The Θ component found for the object is, therefore, improbable for either population type. The result is, however, extremely uncertain. The data are not

inconsistent with Π and Z differing by 20 km/sec or so from the values given and a Θ as low as +40 km/sec.

The proper motion of the south preceding component of the central star, if converted to km/sec at a distance of 2020 pc, is equally improbable. The star's radial velocity is unknown, but it will in any case contribute almost exclusively to the Π component, leaving unchanged the $\Theta = +71$ km/sec and $Z = -86$ km/sec found from proper motion alone. Each of these components is, however, uncertain by as much as 30 km/sec.

The difference between the relative proper motions discussed here and absolute proper motions is uncertain and may, in fact, be negligible. The effect will be, at most, a few per cent of the motions of the individual filaments. The reduction to absolute proper motions is discussed by Trimble (1968).

If this unlikely pair of velocities is to be avoided, then either (a) the mass and geometrical centers of the nebula do not coincide and (b) the star in question is not associated with the nebula or (c) a third, invisible fragment is carrying considerable momentum in the opposite, $-\Theta$, direction.

It has been suggested that this large space motion may be real and the Crab Nebula be a "run away star" from the I Geminorum assocation. There are several reasons for doubting this. The direction of the nebular proper motion makes an angle of 80° with the direction in the plane of the sky from the center of the association to the nebula. The very small radial velocity found for the nebula is

both improbable for an object shot out at random and inconsistent with the large difference in distance between the nebula (at 2.0 kpc) and the association (at 1.5 kpc). Finally, the mass contained in the filaments (Shklovskii, 1966), as well as that of the star if it is a fairly ordinary sort of object at the distance of the nebula, is very much smaller than the masses of most run-aways (Blaauw, 1961).

IV. SUMMARY

Out of this maze of numbers several general conclusions emerge. First, the Crab Nebula is almost certainly located at a distance greater than 1.5 kpc, the balance of probability favoring something around 2 kpc.

Second, the line-emitting filaments are by no means confined to a thin ellipsoidal shell or envelope. For example, (compare Figs. 1 and 2 with the data in Table IV) the faint features numbered 158-160 and 218-225 are all closer than one sixth of the minor axis to the center of the nebula in three as well as in two dimensions. In addition, three stronger features extend more or less radially out of the center. One of these, extending east-west on the east side of the nebula (filaments 161, 172-175, and 206-209), is a superposition of two regions of emitting material at the front and back of the object. A second dark feature, running north-south in the southern part of the nebula (filaments 176-179 and 193) is all on the far side of the object, while the third, running diagonally southeast to northwest toward the preceding edge of the nebula (filaments 183-187, 197-205, and 227) is entirely on the near side. These filaments might be thought of as extending somewhat radially within a thick shell. The adjacent features 194-196 are also close to the center of the object, but on the far side.

For the most part, the expansion is a radial one, each filament having a velocity approximately proportional to its distance from the expansion center. If this were not the case, the filaments would not converge to a single point at a single time in the past. The

largest deviations from this rule of proportionality (300 km/sec and .032"/yr) are five or six times the probable error of the measurements and may be real. Some of these deviations occur in the "bulge" region, but there are a few in all areas of the nebula.

Since one half of the filaments are within about 8" of the expansion center at the date of best convergence (810 years ago), the median deviation from radial expansion must be only about .010"/yr. There are not a sufficient number of data points available near the edges of the nebula to determine a similar quantity for the radial velocities, but the median deviation ought to be something like $4.74 \times 0.010 \times 2020/\sqrt{2}$ or 70 km/sec. These numbers are not significantly larger than the measuring errors, hence the deviations from purely radial expansion cannot be analyzed fruitfully.

The association of the nebula with the so-called central star is neither proved nor excluded, but, if true, it implies an extremely unusual space motion for both objects.

The author is greatly indebted to Dr. Guido Münch, who originally suggested the project, has guided it throughout, and has taken plates especially for it. Thanks are also due to Drs. Jesse L. Greenstein, Richard P. Feynman, and Jan H. Oort who read the manuscript and made many helpful suggestions, and to Dr. Rudolph Minkowski for the loan of observing charts and several illuminating conversations. Conversations with Drs. P. A. G. Scheuer, James E. Gunn, and Jeffrey D. Scargle were also most helpful.

APPENDIX - PROPER MOTIONS OF THE REFERENCE STARS

Table VI lists the coordinates, x and y, proper motions, μ_x and μ_y, and their standard deviations σ_x and σ_y, and approximate magnitudes for the 35 reference stars. The proper motions were determined by comparing each star with the remaining 34 for each of the five base lines 1939-53, 1953-66, 1939-66 (100 in. plates), 1950-64, and 1950-66 (200 in. plates). The values tabulated are the means of the resulting five numbers.

Six of the stars (Numbers 5, 7, 8, 9, 23, and 29) have motions in the x and/or y directions which are larger than three times their standard deviations and are, therefore, probably real. One star has a relative proper motion of about .03"/yr. The others are all .02"/yr or smaller. Neither of the stars used in aligning the plates (A and B in Fig. 1, Numbers 1 and 2 in Table VI) has a detectable proper motion. Of the five stars near the center of the nebula (C through G of Figs. 1 and 4, Numbers 27 to 31 in Table VI), only the south preceding component of the central double star has a motion which is likely to be real.

Magnitudes of the reference stars were estimated by visual comparison with stars of the North Polar Sequence and Selected Area 73 on plates taken by Baade with the 60 in. telescope diaphragmed down to a 40 in. diameter in order to reduce the disturbing effects of the nebulosity. The brightest reference stars were also compared with those stars in the vicinity of the Crab Nebula whose magnitudes are given by Orlova (1966). As can be seen from the table, this was

done in an extremely approximate manner, since the magnitudes were intended for use only in estimating mean parallaxes.

TABLE VI

Star	m_{pg}	X	Y	μ_x "/yr	σ_x "/yr	μ_y "/yr	σ_y "/yr
		"	"				
1	16.5	+ 84.3	- 6.7	+.001	.001	-.001	.002
2	17.5	+170.3	+ 14.4	+.002	.003	+.005	.003
3	17.0	+ 75.3	+ 26.9	-.002	.001	-.005	.004
4	18.0	+ 97.0	+ 91.0	-.001	.002	+.003	.004
5	17.5	+ 79.4	+ 74.8	+.018	.001	-.019	.001
6	18.0	+ 19.5	+103.6	-.003	.002	-.004	.004
7	18.0	+ 15.9	+135.8	-.006	.001	-.005	.002
8	17.5	- 7.5	+109.2	-.005	.001	+.002	.003
9	18.0	- 49.3	+121.8	+.001	.003	+.007	.002
10	18.0	- 82.9	+114.2	-.006	.003	+.006	.004
11	18.0	-102.8	+120.9	-.002	.003	+.007	.004
12	18.0	- 96.9	+ 77.2	+.003	.001	-.007	.006
13	17.5	-164.8	+ 86.9	+.003	.005	+.006	.006
14	17.5	-148.2	+ 52.9	+.003	.005	-.001	.003
15	18.0	-153.7	+ 30.6	+.002	.005	-.002	.003
16	18.0	-107.4	+ 29.1	+.005	.007	+.004	.002
17	16.5	- 82.2	- 69.2	+.004	.004	-.018	.004
18	17.5	- 94.4	-105.6	-.000	.002	-.002	.004
19	18.0	- 61.9	-106.7	-.001	.004	-.002	.002

TABLE VI (Continued)

Star	m_{pg}	X	Y	μ_x "/yr	σ_x "/yr	μ_y "/yr	σ_y "/yr
20	18.0	- 50.3	-118.3	+.002	.001	-.001	.002
21	17.5	+ 29.3	-106.1	-.004	.003	-.005	.002
22	17.5	+ 35.9	- 92.2	-.003	.002	-.001	.002
23	18.0	+ 62.7	- 99.4	-.004	.001	+.006	.001
24	18.0	+152.5	-128.8	-.002	.003	+.005	.007
25	17.5	+166.6	- 98.3	+.002	.005	+.011	.006
26	17.5	+101.3	- 37.5	+.001	.003	-.003	.003
27	17.0	+ 17.4	+ 2.7	+.003	.003	-.006	.003
28	16.0	0	0	-.001	.004	-.001	.007
29	16.0	- 2.5	- 4.2	-.009	.003	-.002	.003
30	17.0	- 0.6	- 14.7	-.001	.002	-.004	.002
31	18.0	- 2.0	- 16.7	-.004	.005	+.001	.004
32	15.5	+ 48.2	- 18.4	+.001	.002	-.009	.004
33	17.5	- 44.0	+ 53.1	+.000	.003	+.002	.004
34	16.0	- 52.9	+ 42.0	-.001	.004	+.004	.003
35	16.0	- 33.6	+ 59.8	-.002	.003	-.006	.003

V. ADDITIONAL DISCUSSION

A. Historical Background

Changes in the appearance of the Crab Nebula were first noticed by Lampland (1921) on plates taken with the 40 in. Lowell reflector. He was reluctant to ascribe them to actual motion within the nebula, perhaps because his plates showed primarily the continuum emission, where some of the changes, if attributed to motions, require very high velocities indeed (Scargle, 1968).

Duncan (1921) immediately measured these changes (on Mt. Wilson 60 in. telescope plates taken by Ritchey in 1909 and himself in 1921) with respect to a group of faint stars. He found that, in the faint outer part of the nebula, the changes take the form of apparent motions of average value .134"/yr in a generally outward direction. He pointed out that this need not imply either an unusual distance or extremely large velocities for the nebula.

This average includes one motion (out of 12) very much smaller than the others, which was found for a feature in the nebula upon which is superimposed a faint star. Duncan apparently measured the star rather than the feature. Removing this spurious motion gives an average of .146"/yr for the features measured, none of which is more than two thirds of the way from the center to the edge of the nebula. The motion at the edges must, therefore, be rather larger. This outward proper motion was interpreted by Hubble (1934) and Mayall (1937) as implying an age of 800 or 900

years for the object.

The first spectra of the Crab Nebula were taken and described by Slipher (1916). Sanford (1919) took additional spectra, correctly identified six of the strongest emission lines, and found velocities of -1000, -600, and +1680 km/sec for three points in the nebula. Neither observer suggested that the displacements of the lines might be due to motion of the emitting material.

Mayall (1937) took spectra along the major and minor axes of the nebula with the Crossley nebular spectrograph. He reported velocities as large as +1650 and -1340 km/sec, but concluded that the maximum rate of expansion was 1300 km/sec and the rate at the center of the nebula only 1050 km/sec. Using that radial velocity and .178"/yr for the angular expansion rate (the average of the seven largest of Duncan's values), he found a distance to the object of 1.5 kpc, which he regarded as an upper limit. He tactitly assumed the object to be an oblate spheroid in doing this.

Duncan (1939) was able to improve considerably the quality of the proper motion measurements by comparing Ritchey's 1909 plate with one taken by himself in 1938. The improvement resulted from the longer time interval between the plates, the availability of a better comparator, and the superiority of the photograph of 1938 over that of 1921. He reported motions for twenty points in the nebula and used them to find the center of expansion (20".3 west and 1".8 south of the north component of the central double star) and the most probable date of the outburst (1172). He weighted all twenty

points equally. Other interpreters of his data (Baade, 1942; Brosche, 1966) find slightly different centers and dates.

Duncan suggested that the present center of the nebula might be the bright region northwest of the central stars which he saw on the earliest of Baade's red-sensitive plates (discussed below). This is a continuum emission feature (the permanent wisp of Scargle, 1968) and is not visible in Figure 1. Using that region for the present center and his expansion center, he found μ_x = -.037"/yr and μ_y = +.005"/yr for the nebula as a whole. This is in the same general direction as, but very much larger than, the present result. Because Duncan used a reference system of faint stars, his measurements have about the same small and uncertain component due to the solar motion which is found in the present results and discussed in section V.C.

Deutsch and Lavdovsky (1940) found proper motions for several features in the continuum emission fairly near the center of the nebula from plates taken in 1896 and 1939 with the astrograph of the Poulkovo Observatory. They confirm a general outward expansion with a time scale of about 800 years.

Radial velocities from a series of nine spectra taken by Mayall (also on the Crossley) are reported by Woltjer (1958). The velocities range from -1190 to +1050 km/sec (with one straggler at +1780 km/sec) and do not seem to tend to zero near the edges of the nebula. Woltjer gives a three-dimensional picture of the nebula constructed from these velocities by Walraven. This picture repre-

sents an extraordinary and seemingly unwarranted extrapolation of the data given. It is somewhat inconsistant with the present results, particularly in the central region of the nebula, where Walraven had no data points whatever to work with.

There are a variety of other spectra of the Crab Nebula taken by various observers at various times in the Mt. Wilson plate collection. None of them approaches the quality of the spectra taken by Münch and Minkowski which were used for the present study. These are described in Part II above.

Direct plates of the nebula were taken with the 100 in. telescope as early as 1924 (Woltjer, 1958), but these, like all the plates used in previous proper motion studies show primarily the continuum emission. In 1939 Baade began a series of 100 in. plates using a red-sensitive emulsion and an RG2 filter to isolate the H_α and nearby [NII] emission lines. An early plate of this series is shown by Baade (1942). He initiated a similar series of 200" telescope plates in 1950. Both series have been continued since his death by Münch.

Although Baade originally intended these plates for a proper motion study, he never measured any of them. His reluctance was due (Münch, private communication) to the fear that the astigmatism (in the case of the 100 in. plates) or coma (in the case of the 200 in. plates) even a few minutes of arc away from the center of the plates would render any such measurements inaccurate. That his fears have proven groundless (as can be seen from the excellent agreement of the results from the two telescopes) is largely a tribute to

the extraordinary skill of the two observers in centering the images on the plates. Coma, of course, becomes much less serious a problem if it is the same for a given star or filament on each plate measured, provided that the exposures are similar. Only four of the reference stars show coma detectable by visual inspection of the plates.

The six plates used in the present study were selected from the two series on the basis of three criteria. These were maximum possible time separation, sharpness of the images, and the desirability of similar densities for all plates to be measured.

B. Accuracy of the Individual Motions, Expansion Center, and Date of Convergence

The uncertainties in both the proper motions and the radial velocities of the individual filaments (given in Tables III and IV) should perhaps be described as "decision error" rather than as "measuring error." Settings on the Grant measuring engine are readily repeatable to within a micron or two, once it has been determined just which feature or part of a feature is to be set on. This choice is, however, not always an easy one to make either for the randomly shaped filamentary features on the direct plates or for the emission lines, many of whose profiles are asymmetric or irregular. The range of possible settings on a given line or filament may, therefore, be from two to eight microns, depending upon its size, shape, and strength. In general, the same decision will not be

made each time a filament is measured on each of several plates nor for each of the emission lines in a given spectrum.

The uncertainties of the motions resulting from this decision process can be seen by comparing the proper motions measured independently on two pairs of direct plates and from the standard deviations of the radial velocities determined from several emission lines.

Figures 7 and 8 are histograms of the data from Table III on the discrepancy of the proper motions determined from the 100 in. and 200 in. telescope direct plates. The quantity E_μ is one half the difference (100 in. μ - 200 in. μ) expressed as a percentage of their average. σ_α is one half of the difference in position angle of the two proper motions (also 100 in. - 200 in.). Note that the signs of both quantities have been kept.

The median difference in length is a bit less than 5 per cent. For a typical proper motion of .1 to .2"/yr, this represents a setting error of from two to five microns in each coordinate on each plate. The proper motions determined from the 200 in. plates are, on the average, about three per cent larger than those determined from the 100 in. plates. This may be the effect of coma on the 200 in. plates. The mean difference in angle is less than 0.1^{o}.

Figure 9 is a histogram of the standard deviations of those 100 radial velocities (from Table IV) which were determined from more than one emission line. The median standard deviation, 14 km/sec, is equivalent to 2.2, 1.1, or 0.6 microns at the disper-

sions involved (110, 215, and 400 Å/mm at λ6500), or a one to five micron uncertainty in the setting on a single line. The two large standard deviations, near 100 km/sec, represent errors in setting on a single line of from 10 to 40 microns, hence the velocities determined from one line may, in a few cases, be extremely uncertain.

As noted in section III.A. above, the filaments for which only proper motions were measured are clustered rather tightly about the expansion center at the date of best convergence. Figures 10 and 11 show the zero epoch positions of the 132 filaments as derived from the 100 in. and 200 in. data respectively. The figures also show the five stars near the center of the nebula, the directions of the major and minor axes in the plane of the sky, and several of the author's thumb prints. The position of the expansion center is marked by arrows near the edges of the figures. For each set of data, one filament lies outside the area shown (not the same filament in each case). The 200 in. data, which are probably more accurate because of the larger scale of the plates, show the positions of the filaments rather more strongly concentrated toward the expansion center than does the 100 in. data. In either case, it is clear that the center cannot be moved more than two or three seconds of arc (the separation of stars F and G) without being obviously wrong.

Figures 12 and 13 are histograms of the dates at which the filaments were closest to the expansion center (assuming constant

velocities) for the 100 in. and 200 in. data respectively. As was the case with the zero epoch positions of the filaments, the scatter is rather greater in the 100 in. data (the arrow indicates that those three filaments really fall off the left end of the date scale) than in the 200 in. data. In each case, the average date of nearest approach to the center is clearly later than 1054, and there is no question that the observed acceleration is real.

The amount of that acceleration (as calculated in section V.D. below) does not depend directly on the date of convergence, but only upon the maximum proper motion found. Since that maximum proper motion must be (for a given length of the major axis) inversely proportional to the apparent age of the nebula, it can be shown that an error of twenty years in the convergence date will produce an error of about 20 per cent in the value found for the acceleration (and hence in the forces involved in producing it).

Analogies to Figures 7-8 and 10-13 can be constructed from the proper motion data of Table IV. They show rather larger scatter (because these features could not be chosen for ease of measurement) but are otherwise similar.

C. Reduction to Absolute Proper Motions

The proper motions discussed above for the individual filaments, the nebula as a whole, and the central star are relative to a group of faint stars and include some component due to the solar motion. If the nebular motions had been measured with respect to

group of objects at infinite distance, then (assuming a distance of 2.02 kpc to the nebula) they would contain a component of .0022"/yr in position angle $139^{\circ}45'$ due to the reflex of the basic solar motion. In fact, many of the reference stars may be closer than the nebula, and measurements made against such a "background" will also contain a component in the opposite direction, position angle $319^{\circ}45'$. This latter component will be equal to the mean secular parallax of the reference stars.

Mean parallaxes for faint stars as a function of galactic latitude and magnitude are available from two sources. A tabulation due to Binnendijk (1943) extends to $14^{m}.7$ and excludes stars of large proper motion. The values in this table are, therefore, rather smaller than those given by van de Kamp (1941) who did not exclude large proper motions. The latter list extends to $16^{m}.0$. Each list has been extrapolated to $18^{m}.0$ by assuming that the luminosity function near the sun (van Rhijn, 1965) continues to be valid out to several kiloparsecs. Absorption of $1^{m}.0$ per kpc was assumed. Mean secular parallaxes as a function of magnitude for galactic latitude -6° from these two sources and their extrapolations are listed in Table VII. The smaller values, given by Binnendijk, are the more likely to be applicable, since there are no stars with large proper motions in the reference group.

TABLE VII*

MEAN SECULAR PARALLAXES OF FAINT STARS
FOR GALACTIC LATITUDE -6°

	Mean Secular Parallax	
m	Binnendijk	van de Kamp
14.0	0".0052	0".0081
14.7	.0047	---
15.0	(.0044)	.0074
15.5	(.0036)	(.0072)
16.0	(.0033)	.0069
16.5	(.0029)	(.0067)
17.0	(.0026)	(.0065)
17.5	(.0023)	(.0064)
18.0	(.0021)	(.0063)

*Values in parentheses are obtained by extrapolation as described above.

Combining the data from Tables VI and VII gives a mean secular parallax for the 35 reference stars of either .0024" or .0064". A component of either .0002"/yr or .0042"/yr in position angle $319^{\circ}45'$ should, therefore, be subtracted from all of the proper motions recorded for the nebula in order to obtain absolute proper motions.

If the larger value of the mean secular parallax is more nearly correct, the effect upon the motions of the individual filaments

will be, at most, a few per cent, or no larger than the measuring errors. The proper motion of the nebula as a whole will be reduced to μ_α = -.009"/yr and μ_δ = +.0073"/yr or a total of .0073"/yr (70 km/sec at 2.02 kpc) in position angle 353°, and that of the south component of the central double star to μ_α = -.006"/yr and μ_δ = -.005"/yr or a total of .008"/yr (78 km/sec) in position angle 232°. In Figure 4, the 1054 positions of the star and the nebula (i.e. the expansion center) would each be moved about 3".5 to the northeast if the larger mean parallax is correct. Their separation is not changed, hence the strength of the evidence for their physical connection is unaffected.

If, as seems most probable, the smaller value of the mean secular parallax is correct, the effect is entirely negligible, and the motions found for the individual filaments, the nebula as a whole, and the central star are, in fact, absolute proper motions (subject to the many reservations about the validity of the latter two motions discussed above).

D. Interpretation of the Acceleration and Deviations From Radial Motions

In accordance with Newton's first law of motion (Newton, 1686) matter expelled by a supernova explosion ought to move at constant speed in a straight line. Any deviation from this pattern requires some explanation.

A slight slowing down of the expansion might readily be

attributed to interaction with the interstellar medium, but this is not the effect which is found. As noted in Section III.A. above, if the present expansion of the nebula is extrapolated backward in time, the object converges to a point in about 1140, much later than the supernova event in 1054. The expansion, therefore, has been accelerated.

If this acceleration is assumed to have been constant over the history of the nebula, then its magnitude may be found from the equations,

$$S = at + bt^2$$

$$\frac{dS}{dt} = a + 2bt$$

where S is the semi-major axis of the ellipse in the plane of the sky (180"), t is the true age of the object (1950 - 1054 = 896 years), and dS/dt is the present maximum expansion rate (.222"/yr). The acceleration is then .000023"/yr^2 or .00073 cm/sec^2 for a distance of 2.02 kpc. If the acceleration all occurred during the early phases of the expansion, it might, of course, have been much larger.

Baade (1942) attempted to account for this acceleration in terms of radiation pressure from an assumed central star of radius 1.4×10^9 cm and temperature 5×10^5 degrees. The momentum transferred to the gas by the radiation from such a star is too small by a factor of at least 10^3 to explain the observed acceleration, even if the nebula is assumed to be optically thick at all wave lengths (which it clearly is not, since we see line-emitting filaments on the

back side of the object). The radiation from even a very hot white dwarf or neutron star is similarly inadequate. In fact, a star emitting sufficient radiation to produce the observed acceleration would have an apparent bolometric magnitude of about +5, very much brighter than any star in the vicinity of the nebula.

Woltjer (1958) points out that both the magnetic field and the relativistic particles (which produce the synchrotron continuum emission from the nebula) exert a force tending to accelerate the expansion. It can be shown that, to within the uncertainties of the various quantities involved, either or both of these mechanisms is sufficient to produce the observed acceleration. Unfortunately, none of the required quantities (the total mass, the total relativistic particle energy content, and the average magnetic field of the nebula) can be estimated in a manner completely independent of the distance or one of the other required quantities.

The mass of the nebula was found to be about 0.1 solar mass by Osterbrock (1957) and Woltjer (1958). This must be increased to .3 or .4 solar mass if the distance is 2 kpc.

The total energy of the relativistic particles must similarly be increased from the 2.4×10^{47} ergs found by Shklovskii (1960) or the 7×10^{47} ergs found by Woltjer (1958) to about 2×10^{48} ergs. The value found for this total energy is, in either case, inversely proportional to that assumed for the magnetic field.

Pikelner (1956) has estimated the magnetic field from the frequency at which the radio spectrum bends over to join the optical

spectrum. This frequency depends somewhat on the visual absorption (and hence on the distance) assumed. He finds a field of 3×10^{-4} gauss over the nebula as a whole and a maximum near the center of 5×10^{-4} gauss. A value near 3×10^{-4} also follows from setting the magnetic energy density equal to the energy density of the random mass motions (Shklovskii, 1960), but this is dependent upon the choices of the mass, distance, and magnitude of the random velocities. The values used were .4 solar mass, 2 kpc, and 200 km/sec, all rather different from those suggested by Shklovskii.

All these numbers form a consistent system. If the acceleration is attributed to particle pressure, then a total relativistic particle energy content of 2×10^{48} ergs distributed in a region of radius 3.6×10^{18} cm (2 minutes of arc at a distance of 2 kpc) will exert a total force of 5.5×10^{29} dynes, sufficient to impart the observed acceleration (.00073 cm/sec^2) to a mass of 8×10^{32} grams or .4 solar mass. Johnson and Townes (1957) have shown that a flux of relativistic particles continuously emitted from a central star can also produce the observed acceleration.

If the acceleration is attributed to magnetic pressure, then the pressure, $2H^2/8\pi = 10^{-8}$ dyne/cm^2, due to a magnetic field of 4×10^{-4} gauss is sufficient to impart the observed acceleration to a column of unit cross-section through the nebula containing 1.4×10^{-5} gram. This is equivalent to a total nebular mass of about .2 solar mass. A superficially similar calculation given by Ginzberg and Syrovatskii (1964) is in error because it assumes that the accelera-

tion occurs only along the major axis of the ellipse and must, therefore, be due to an anisotropy of the magnetic field. As a result, they estimate from the observed acceleration an average field which is too large by a factor of almost ten.

Burbidge (1958) finds a much larger magnetic field ($\geq 10^{-2}$ gauss) and total particle energy (5×10^{50} ergs) by regarding the relativistic electrons as the secondaries of a large flux of relativistic protons. These large values do not fit in with the consistent pattern of field strength, energy, mass and acceleration just found, which indicates that the electrons cannot be secondaries.

The observed acceleration of the nebular expansion may be regarded as being satisfactorily explained by either relativistic particle pressure or magnetic pressure or both.

Deviations from uniform straight line motion have also been noted in section III.A. above. Two quantities provide a measure of these deviations. They are $100\% \times (r - \mu t)/r$, where r is the distance in the plane of the sky of the filament from the center of the nebula and t is the apparent age of the nebula, 810 years, and $(\tan^{-1} y/x - \tan^{-1} \mu_y/\mu_x)$ expressed in degrees, where x and y are the coordinates and μ_x and μ_y are the proper motions of the filament. The values of μ, μ_x, and μ_y can be taken directly from Table III and the values of r, x, and y computed from Table III using the coordinates of the center given in Table V. The two quantities may be described as (1) the difference between the true central distance of a filament and the central distance it would have

had if its speed had been constant over the age of the nebula, divided by the true central distance and (2) and angle between the radius vector to the filament and its present direction of motion. If the nebula had moved radially outward with uniform acceleration, both these quantities should be zero for all filaments, to within the accuracy of the measurements.

Figures 14 and 15 show the number of filaments having given values of the two quantities. These figures should be compared with Figures 7 and 8 which represent the uncertainty of the measurements and are drawn to the same scale. The striking similarity of the two pairs of figures may be taken to indicate that virtually all the apparent deviations from uniform radial expansion are due to measuring errors. This conclusion is strengthened by the fact that for both the zero-epoch positions of the filaments and for the dates at which they were nearest to the expansion center, the scatter of the (presumably more accurate) 200 in. data is rather less than that of the 100 in. data. (See Figs. 10 - 13.) The apparent scatter in these positions and dates are, of course, a direct result of the apparent deviations from uniform expansion.

The radial velocity results are not quite so clear in this respect. It is, of course, not possible to say in general whether the radial velocity of a given filament is precisely appropriate to its position along the line of sight or not, because that position can only be determined as the product of the velocity and the age of the nebula. On the other hand, since in the plane of the sky the filaments

are confined so closely to an ellipse, it is extremely likely that in three dimensions they are confined within the ellipsoidal surface

$$\frac{x^2}{a^2} + \frac{y^2}{b^2} + \frac{z^2}{b^2} = 1$$

where x and y are coordinates along the major and minor axes in the plane of the sky, z is the coordinate along the line of sight, and a and b are the semi-major and semi-minor axes (5.4 and 3.6×10^{18} cm for a distance of 2 kpc). Thus the largest z a given filament should have can be found from its x and y position. Any velocity excess, ΔV, given by

$$\Delta V = \left| V_r^{\text{observed}} - \frac{z}{\text{age}} \right|$$

must then be of the same nature as the quantity $r - ut$ discussed above, except that it will be only a lower limit since we have only an upper limit to z.

Such a velocity excess is found for ten of the features in Table IV, five on the front ($V_r < 0$) and five on the back ($V_r > 0$) of the nebula. These are listed in Table VIII.

TABLE VIII

RADIAL VELOCITY EXCESSES

Filament	V_R	σ_V	ΔV
140	+1382	--	26
180	- 879	2	879
181	- 732	8	732
182	- 217	50	217
189	- 960	--	17
190	+ 716	9	64
220	-1482	44	61
239	+1313	--	6
246	+1647	--	315
247	+1470	--	192

Three of the velocity excesses (180-2) are in the region of the bulge on the south preceeding edge of the nebula and are probably not relevant to the problem at hand. It should be noted that this bulge is located adjacent to one of the two "bays" in the continuum emission where (as discussed by Scargle, 1968a) the magnetic field configuration is such that particles ought to be able to leak outside the nebula.

Five of the remaining seven excesses are of unknown accuracy because the radial velocity was determined from a single line. In

view of this, measuring errors even as large as 200 or 300 km/sec (filaments 246-7) cannot be ruled out. The very much smaller excesses for filaments 140, 189, and 239 are still less distinguishable from the uncertainties of the measurements. The remaining two excesses are of the order of 60 km/sec with standard deviations of 9 and 44 km/sec. Although these are lower limits, the existence of real deviations from uniform expansion does not seem to be established.

This is in no way contradicted by the velocities reported by Woltjer (1958), although a few of them appear to be both rather large and rather near the edge of the nebula. His finding chart does not show the faint filaments which mark the true edge, and it should be recalled that a feature need be only 3" in from the extreme end of the major axis in order that z/age = 300 km/sec.

The evidence of both the proper motions and the radial velocities therefore indicates that apparent deviations from purely radial motion are largely or wholly due to the inaccuracies of the measurements.

Greenstein (1968) has suggested that part of the apparent deviations from purely radial expansion might be the effect of wave motion in the nebula. If, for example, an outward-moving filament were to encounter a region of increased magnetic field not parallel to its motion, then an Alfven wave should run along the field lines giving the appearance of non-radial motion.

Wave propagation in the medium outside the filaments has

been discussed extensively by Scargle (1968). He finds that both the Alfven velocity and the speed of sound are several per cent of the speed of light in the low density regions of the nebula. Since the deviations from radial motion are, at most, a few hundred km/sec, wave motion in the low density regions cannot explain them, although it seems to be an important cause of the changes observed in the continuum radiation.

The relevant velocities are, of course, very much smaller within the filaments. For a temperature of 10^4 (Woltjer, 1958) and a composition varying from pure helium to pure hydrogen, the speed of sound is 10 to 20 km/sec.

The Alfven velocity will be in the same range for reasonable values of the density and magnetic field. The electron density in the stronger filaments is of the order of 10^3 to 2×10^3 particles per cm^3 (Osterbrock, 1957; Woltjer, 1958). As discussed above, the magnetic field is of the order of 3 to 5×10^{-4} gauss. For these values of the density and magnetic field strength, the Alfven velocity is between 15 and 35 km/sec or .001 to .003"/yr at the distance of the nebula. This is too small to explain the observed non-radial motions in the "bulge" region as well as too small to be distinguished from the inaccuracies of the measurements.

Any expansion or disturbance of the individual filaments will move at these characteristic speeds and will take several hundred years to travel 1" in the plane of the sky. This partially accounts for the fact that the smallest features seen in the emission

lines are readily traced over a period of 30 years.

E. Reliability of the Distance Determination

None of the non-dynamic arguments given in section III.B. to support a distance to the Crab Nebula of about 2 kpc is individually very strong, although in combination they remain reassuring in the absence of any contrary arguments.

Woltjer (1958) notes that his results involving line ratios can be explained by an anisotropic radiation field as well as by doubling the assumed distance (from 1.03 to 2.06 kpc). An intermediate distance of 1.5 kpc would also explain his observations while remaining consistent with the assumption that the nebula is an oblate spheroid.

Poveda and Woltjer (1968) have indicated that the interstellar magnetic field is much too weak to affect the shape of the nebula by directly guiding the present expansion. They suggest, however, that the field might have influenced the motion of matter ejected before the supernova event, causing it to accumulate in such a way that the supernova shell could less easily expand transverse to the original field direction. It seems, on the other hand, at least equally probable that any pre-supernova material should have been strung out along the direction of the field lines allowing the shell to expand preferentially in a transverse direction. If the interstellar magnetic field is not parallel to the galactic equator near the Crab Nebula,

the argument cannot apply in any form.

It has already been noted that, if the supernova of 1054 was not a Type I event, then its maximum brightness cannot be used to find its distance.

As Shklovskii (1966) has suggested, some novae seem to eject matter preferentially along a polar axis. Other novae do not.

Finally, although increasing the distance, and hence the interstellar absorption, changes a variable spectral index to a constant one in the millimeter, infrared, and optical regions, it changes a constant spectral index to a variable one in the soft X-ray region. The size of this effect can be estimated.

Felten and Gould (1966) show cross-sections per atom of neutral hydrogen for the absorption of X-rays by the interstellar medium, assumed to have the composition given by Aller (1961). Radio data (Clark et al., 1962) indicate that there are about 1.5×10^{21} atoms of hydrogen per square centimeter (distributed in several clouds) between the sun and the Crab Nebula if it is at a distance of 1.1 kpc. The optical depth, τ, of the interstellar medium between the sun and the nebula is then about .58 for photons of 1 kev energy, .08 at 2 kev, .03 at 3 kev, and .01 at 4 kev. The number of hydrogen atoms between us and the nebula can also be estimated from the data on the galactic distribution of hydrogen given by Schmidt (1957). This gives a very similar result for a distance of about 1 kpc, while the values of τ out to 2 kpc are 1.3 for photons of 1 kev energy, .19 at 2 kev, .07 at 3 kev, and .03 at 4 kev.

Table VIII gives the emitted flux densities, F^{em}, for these two sets of optical depths. The observed fluxes, F^{obs}, are taken from Grader et al. (1966) and Haymes et al. (1968). α is the spectral index of the emitted radiation. The effect of allowing for some absorption is to make the spectrum rather steeper at the lowest X-ray energies measured, as shown in Figure 16 (taken from Haymes et al., 1968).

If the smaller distance is correct, the effect is slight and the continuity of the X-ray with the optical spectrum is not seriously disturbed. If the larger distance is correct, then the emitted X-ray flux is rather too great to be smoothly connected with the optical flux, even if the visual absorption is quite large. Such a discontinuity suggests that the X-radiation may have an origin different from that of the optical radiation. This possibility is discussed by Williams (1967) in connection with his prediction of emission line intensity ratios in the nebula. A separate origin for the X-rays would account for the large discrepancies between observed and predicted line ratios, since the flux of ionizing ultraviolet radiation could then be much smaller than what is obtained by drawing a straight line between the observed optical and X-ray fluxes. The variable spectral index of the X-radiation implied by the larger distance ceases to be objectionable if the radiation has a separate origin.

The numbers obtained by setting proper motions equal to radial velocities therefore remain the only firm handle on the distance to the Crab Nebula.

TABLE VIII

OBSERVED AND EMITTED FLUX DENSITIES OF THE CRAB NEBULA IN THE SOFT X-RAY REGION

		Distance = 1 kpc			Distance = 2 kpc		
Energy kev	Log F^{obs} watt/m^2-HZ	τ	Log F^{em} watt/m^2-HZ	α	τ	Log F^{em} watt/m^2-HZ	α
1	-28.13	0.585	-27.87	2.0	1.30	-27.57	3.0
2	-29.49	0.084	-28.45	1.6	0.19	-28.41	2.0
3	-28.71	0.030	-28.70	1.3	0.067	-28.68	1.5
4	-28.85	0.015	-28.84	1.2	0.034	-28.83	1.2
≥ 5	---	≤ 0.010	unchanged	1.2	≤ 0.010	unchanged	1.2

F. Ionization and Excitation in the Filaments

Variations of the intensity ratios of various emission lines have been reported in the Crab Nebula by Minkowski (1942b) and Woltjer (1958) and in other supernova remnants by Parker (1964b). Three factors interact to produce these ratios and their variations. They are the abundances of various elements, the density of the emitting gas, and its temperature (that is, the degree of ionization and excitation).

It is customary to attribute unusual spectra to unusual abundances only as a last resort, and it is, indeed, possible as discussed below to explain the main features of the line emission spectrum of the Crab Nebula in terms of standard abundances of the metals as given, for example, by Aller (1961). This does not mean, however, that these standard abundances must be correct for the nebula, since the interpretation of the spectrum is by no means unique.

In the case of the Cygnus Loop, it has been pointed out (Parker, 1964b) that any enrichment in metals or helium of the material expelled by the supernova must have been diluted by a factor of about one hundred to one by the interstellar matter swept up by the expanding shell. This is not the case with the Crab Nebula. The total mass of the object (as discussed in section V.D) is of the order of 0.4 solar mass, while the amount of interstellar matter (if it has an average density of 0.1 atom/cc) swept up during the expansion must be only about 0.1 solar mass. Thus any abundance anomalies in the matter ejected by the supernova should have been preserved. The helium to

hydrogen ratio, discussed below, is probably larger than that found for most planetary nebulae and early type stars.

Line intensity ratios are, of course, best determined photoelectrically. The present material, both spectra and direct plates, can, however, be used to obtain approximate line ratios. Although no calibration plates for wavelength sensitivity are available for the spectra which were measured for radial velocities, the Hα/[NII] ratio can be determined rather easily since the lines are very close together. The Hα/[SII] and Hα/[OI] ratios can be found approximately by taking account of the sensitivity curve of the Kodak 103a-E plates on which the spectra are recorded.

Among the 200 in. plates taken by Baade is one for which a 103a-F plate and an RG5 filter were used to isolate the red lines of [SII]. The degree to which such a plate will be contaminated by Hα and [NII] is estimated by Woltjer (1958). The contamination may be as large as 50%. It will also be extremely variable, depending both on the line ratios in a particular filament and on the radial velocity of that filament. Any quantitative conclusions drawn from such a plate must, therefore, be extremely uncertain. A 200 in. plate in the light of [OIII] was taken by Münch using an interference filter of about 100 Å bandpass centered at λ 5000. The wide bandpass is necessitated by the large velocity dispersion in the Crab Nebula. The contamination in such a plate is very much less than when only a color filter is used. Even the continuum is very faint. In addition, 48 in. Schmidt telescope plates of the nebula have been taken through

interference filters centered on [OI] λ6300, [OIII] λ5007, Hβ, and [OII] λ3727 by the present author. The Hβ filter was so narrow that it excluded many features of high radial velocity and no impression of the appearance of the nebula in Hβ can be gained from a plate taken through it.

Sensitometric calibration plates made with the wedge spectrograph in the 200 in. dome exist for all of these. In addition, 48 in. Schmidt plates have been taken through each of the four interference filters of two planetary nebulae whose line emission intensities have been measured photoelectrically by Collins, et al. (1961). It was intended that these plates be used for quantitative measurement, but in view of their small scale and the unsuitability of the calibration of the absolute intensities, the main properties of the nebular emission were determined from simple inspection of the plates. As a result, changes in line ratios are very much better determined than the values of the ratios themselves.

Several calculations have been made of the line intensity ratios to be expected from nebular material at densities and temperatures appropriate to the Crab Nebula. Various ionization and excitation conditions have been assumed.

Burbidge and Burbidge (1962) have considered the case of a diffuse nebula ionized by diluted stellar radiation. The excitation of the metastable states of N^+, O^+, and S^+ is collisional; the excitation of hydrogen is radiative at $10,000^o$ and collisional at $20,000^o$ and $40,000^o$. They find that the ratios of Hα to each of the three for-

bidden doublets are all strongly decreasing functions of temperature.

Parker (1964a,b) calculated both absolute and relative intensities of $H\alpha$, $H\beta$, and the forbidden doublets of N^+, O^+, O^{++}, and S^+ for a nebula under conditions of collisional excitation and ionization. All the ratios are quite sensitive to temperature except $H\alpha/[NII]$ at temperatures above $20,000^{\circ}$.

Williams (1967) has predicted line ratios of $H\alpha$, [OII], [OIII], and several helium and neon lines for the case of a plane parallel gas slab of finite thickness illuminated from one side by synchrotron radiation of spectral index 1.1 and compared them with the observed ratios given by Woltjer (1958).

The reverse procedure was carried out by Woltjer (1958) who used the observed line ratios to find temperatures and abundances in the nebula and the spectral index of the illuminating radiation.

In all cases, near an electron density of 10^3 (such as was found for the Crab Nebula by Osterbrock (1957) from the ratio $\lambda 3726/\lambda 3729$ of [OII], which depends strongly on density and weakly on temperature) the intensities of the lines of hydrogen and helium as well as of the forbidden doublets are all nearly linear in density. The line intensity ratios are, therefore, virtually independent of density.

In order to discuss the observations, it will be necessary to assign names to some of the more prominant features of the nebula, as sketched in figure 17. The three strong filaments described in section IV will be known as filaments I, II, and III respectively. The band of strong emission extending northeast from III to the large U-

shaped feature due north of the central double star will be known as IV, the U itself as V, the strong feature to the east of V as VI, and that to the west of V as VII. The regions containing no strong emission at the south and north ends of the major axis will be known as VIII and IX respectively. The "bulge" region and the center of the nebula do not seem to require further identification.

The first observation is largely a negative one. There seems to be no correlation one way or the other between the distribution of the continuum emission (as shown, for example, by Oort and Walraven, 1956) and the distribution of the filaments, except that there are no strong filaments very near the center of the nebula where the continuum activity (described by Scargle, 1968) is concentrated. The eastern portion of feature I seems to bisect the "bay" in the continuum emission on the east side of the nebula. Judging from the radial velocities (filaments 149, 150, and 156 of Table IV and figure 3), the feature lies rather close to the outside of the nebula in three dimensions, away from the region of strong continuum emission (assuming that the continuum emission is confined, like the filaments, to a prolate spheroid). The symmetric position of this feature with respect to the bay is, therefore, evidently accidental.

Some of the strongest features (but not IV or VI) are approximately parallel to the direction of polarization of the continuum radiation (as shown by Woltjer, 1958) at their positions. The "bulge" is located at a point where the magnetic field lines (shown by Oort and Walraven, 1956) extend almost radially out of the nebula in the plane

of the sky. It seems likely that the "bulge" is the result of leakage of particles along these field lines. If the field lines are not parallel to the plane of the sky, this would also account for the rather large radial velocities noted in section V.D for filaments in this region.

The [OI] line at λ6300 is the weakest of those observed and has been very nearly lost from figure 2 in the reproduction process. It can be seen on the spectra in features I - V and VII only where the other lines are very strong. In a few cases, the line is as strong as the weaker of the two [NII] lines. This generally occurs where the ratio Hα/[NII] is the largest. The direct plate in the light of [OI] shows the same six features and very little else. Feature VI is completely absent. Parts of the continuum are as strong as any of the filaments on this plate.

Although the [SII] lines, λλ6711 and 6728 are readily visible on all spectra, they fall at a point where the sensitivity of the plates is dropping rapidly. Their apparent weakness relative to [NII] in figure 2 is, therefore, quite consistent with Woltjer's comment that [SII]/[NII] can be as great as 1.4. In addition, the radial velocity of a filament will strongly influence the density on a spectrum produced by a given emitted intensity in these lines. If one allows for these factors, the observed ratios then vary from rather less than one to about two. The direct plate in the light of [SII] is quite surprisingly different from figure 1. Region VIII is greatly enhanced, as is feature II. The west part of I and the east part of III are strong, while the east part of I, the west part of III, all but the southern part of IV, and

the bulge are completely absent. VII is very weak. For the most part, [SII] tends to be strong where Hα/[NII] is large, and weak where Hα/[NII] is small.

The two [NII] lines ought (Garstang, 1951) to be in the ratio $\lambda 6583/\lambda 6548 = 3$, and, as expected, there are no conspicuous deviations from this. Hα, on the other hand, varies from being stronger than $\lambda 6583$ to being weaker than $\lambda 6548$. This means that Hα/[NII]$_{\lambda 6583 + \lambda 6548}$ ranges from greater than one to less than one-fourth. The ratio is about one in region VIII, feature II, and the parts of I and III nearest the center of the nebula. These are the features in which [SII] was strong. (None of the spectra shows region IX.) The ratio is equal to or less than 0.25 in features IV and VII, the east part of I, the west part of III, and the "bulge" (where H is completely absent). These are also the regions in which [SII] was weak or absent. The ratio in the other strong features and in the weak filaments near the center of the nebula is about 0.5.

The ratio of the doublets [OIII]/[OII] is also quite variable. Woltjer (1958) gives a mean value for the ratio of 1.5 with a range of 0.57 to 2.4. This is confirmed by direct plates in the lines. Using interference filters of similar band pass, similar exposure times produce plates of similar density in the two pairs of lines. Since the 103a-J emulsion is less sensitive at $\lambda 5000$ than is the 103a-O emulsion at $\lambda 3727$, the [OIII] emission is evidently the stronger.

The plates look quite different from each other as well as from figure 1 and the [SII] and [OI] plates. [OIII] is particularly strong

in the eastern part of feature I, the northern part of II, the western part of III, the southern part of IV and the faint features in the central region. These are precisely the features which, according to the radial velocity data, are close to the center of the nebula in three dimensions. [OII] predominates in the other strong features as well as in regions VIII and IX and the "bulge."

Woltjer's measurements of the intensities of the lines λλ3889 and 4471 of HeI and λ4686 of HeII also indicate that the higher ionization state predominates in those features physically near the center of the nebula, while HeI is strongest in the outer regions.

Ratios involving the intensities Woltjer gives for the Balmer lines, the [SII] doublet near λ4075, and the [NeIII] lines λλ3869 and 3968 vary in a fashion consistent with the stronger lines. That is, for those few points in the nebula common to his observations and the present ones, the higher members of the Balmer series are strong where Hα/[NII] is large, the violet [SII] doublet is strongest where the direct plate in the red [SII] doublet shows the most emission, and [NeIII] is enhanced in the same regions as [OIII].

The calculations of both Woltjer and Williams show that the ratio of Hβ to λ4471 of HeI is much more sensitive to abundance than to temperature or the spectral index of the ionizing radiation. Both authors find that the mean ratio of the lines, Hβ/λ4471 = 5.4, implies a helium to hydrogen ratio of about 0.45 by number. The observed ratio of the lines in various filaments, however, ranges from less than three to about nine. Changing the electron tempera-

ture by a factor of two (8,000° to 16,000°) or the spectral index of the ionizing radiation by almost a factor of two (1.1 to 2.0), on the other hand, changes the expected line ratio by a factor of only 1.5.

If Woltjer's observed line ratios are not seriously in error, there must be real composition differences among the filaments. Nuclear reactions in supernova events and the probable over-abundance of He in the Crab Nebula are discussed by Greenstein and Minkowski (1953). Lithium and carbon, but no extra helium, may be produced by the supernova itself. The helium enrichment of the nebula is, therefore, somewhat surprising, since, if the 0.4 solar mass found in the nebula had been blown from only the outer layers of a star, the He/H ratio in the ejected matter should have been unaffected by nuclear processes. The average He/H ratio of 0.45 for the nebula nevertheless indicates that some enrichment has occurred. The interstellar matter swept up by the expanding nebula will almost certainly have had normal abundances. The variability of line ratios then means that the helium-enriched ejected matter and the helium-poor swept up matter have not been thoroughly mixed. This non-mixing is quite consistent with the long periods of time over which individual filaments maintain their identity.

Because the lines of different ions arise in different parts of the nebula, a temperature derived from average line intensities will not apply to any specific region of emitting gas, nor can the temperature be determined independent of an assumed composition in the case of line ratios involving two elements. Fortunately, an approximate

electron temperature can be derived from the ratio of the [OIII] lines ($\lambda 4959 + \lambda 5007)/\lambda 4363$ which will not suffer from either of these problems. Woltjer adopts a mean value of $17,000^{o}$ for the temperature obtained from this ratio. His data indicate a range of from $14,000^{o}$ in some of the stronger features (those parts of I, II, and III physically near the center of the nebula) to about $27,000^{o}$ in the faint outer filaments.

Electron temperatures of this order rule out both collisions and blackbody-like radiation as the source of ionization. The nearly equal intensities of the [OII] and [OIII] doublets require nearly equal amounts of the two ions. This implies a temperature near $40,000^{o}$ if the ionization is collisional (Parker, 1964a) and even higher if it is due to black body radiation (Burbidge and Burbidge, 1962).

This leaves the synchrotron radiation of the nebula itself. The important difference between the two kinds of radiation in this context is the number of quanta of uv radiation present relative to a given intensity of optical radiation. A synchrotron spectrum is much flatter than a black body spectrum. That is, there are many more photons capable of producing O^{++}, He^{+}, N^{++}, and the like (250 - 550 Å) available.

Woltjer finds that, in order to produce the observed [OIII]/[OII] ratio, the ionizing radiation must have a spectral index of about 1.5 from 4250 Å to 250 Å. This is steeper than the spectral index of the optical radiation or the X-radiation considered separately. It is also steeper than the spectral index (about 1.1 - see figure 16) found by

drawing a straight line between the optical and X-ray fluxes, even if there is no interstellar absorption of X-rays. If some absorption must be allowed for, the larger emitted flux in the soft X-ray region implies also a larger emitted flux of the ultraviolet ionizing radiation if it is to fall on the line drawn between the optical and X-ray fluxes.

Williams (1967) adopts a spectral index of 1.1, thereby overestimating the flux of ionizing radiation by a factor of about four. (His value of the flux at λ4250 is also different from that used by Woltjer.) He indeed finds [OIII]/[OII] = 5.3, also too large by about a factor of four. The degree of ionization of nitrogen is probably similarly overestimated, N^{++} gaining at the expense of N^{+}.

Williams' overestimate of the flux of ionizing radiation has a second effect. According to his calculations, the radiation field of the nebula is sufficient to maintain an electron temperature which varies from 13,000° to 10,000° across a typical filament (the side toward the center of the nebula being the hotter), while according to Woltjer some additional source of heating is required. He suggests collisions with interstellar atoms, radioactive matter in the filaments, or a strong far-ultraviolet radiation field from the central star. The present observations show that the first of these is probably the most important.

The [OI] line is so weak that it could not really be determined where it is enhanced or weakened with respect to the other lines. As a result, very little information can be derived from it. The line appears in all but one of the strong features (VI). Its intensity is

probably quite dependent on density for two reasons. Higher density will both increase the frequency of recombinations and increase the optical depth in the Lyman continuum, thereby depleting the supply of radiation capable of ionizing neutral oxygen (I.P. = 13.56 ev.). For what it is worth, Woltjer's method of deriving the density from the surface brightness in Hβ was applied to his single data point in feature VI and indeed gives an electron density (about 600/cc) slightly lower than any found by Woltjer (1958) and comparable with the lowest found by Osterbrock (1957).

For electron temperatures of the order of $10,000^{o}$, the ratio Hα/[SII] varies directly with temperature while Hα/[NII] varies inversely with temperature for a given degree of ionization (Parker, 1964a). It may, therefore, be concluded that those regions of the Crab Nebula in which [SII] is enhanced and Hα/[NII] is large are cooler than those regions in which [SII] is weak and Hα/[NII] is small.

The electron temperatures required will depend upon the degree of ionization. The mean ratio N^{+}/N can be estimated at 0.5 from the data given by Williams (1967) if it is assumed that his N^{++}/N^{+} ratio is too large by the same amount as his O^{++}/O^{+} ratio, due to the choice of spectral index 1.1 for the ionizing radiation. The observed range of Hα/[NII] (about 0.2 to 1) will then be produced by electron temperatures ranging from $8,000^{o}$ to $20,000^{o}$, if the N/H ratio is taken from Aller (1961). This is rather lower than, but quite consistent with, the range of temperatures found from

the [OIII] lines. A large N/H ratio would give lower temperatures. The result is much the same whether the formulae for forbidden line strengths are taken directly from Seaton (1954) or Woltjer's approximations are used.

If the mean degree of ionization of sulfur is also like that of oxygen and nitrogen, the ratio of [SII]/[NII] will vary from 2.0 to 0.7 over a temperature range of $10,000^{o}$ to $17,000^{o}$ for a normal S/N ratio. Both these temperature ranges will be affected by variations in ionization such as are indicated by the variable [OIII]/[OII] ratio.

In general, [SII] is enhanced and [NII] weakened relative to $H\alpha$ in the inner parts of the nebula where the gas is most highly ionized (those parts of features I, II, and III and the faint filaments near the center of the nebula). Conversely, [SII] is weak and [NII] strong with respect to $H\alpha$ in those strong features well away from the center of the nebula in three dimensions and in the bulge where the gas is least highly ionized. This means that the range of temperatures required to explain the $H\alpha$/[NII] ratio is somewhat narrowed and that required to explain the [SII]/[NII] ratio somewhat broadened. A single range of about $9,000^{o}$ to $18,000^{o}$ can therefore account for the concomitant variation of these two line ratios. The only exception to this general pattern is region VIII which is evidently an area of both low ionization and low electron temperature.

The general pattern suggests very strongly that the primary source of ionization is the synchrotron radiation coming from inside the nebula, while the primary source of excitation and heating is

collisions with the interstellar matter on the outside of the nebula. This latter is confirmed by the Hα/[NII] ratio in feature VI which is a superposition of two emitting filaments on opposite sides of the nebula. The material on the far side of the nebula (filaments 229-232 of Table IV) has a mean radial velocity of +490 km/sec and is therefore much closer to the outside of the nebula than is the material on the near side (filaments 233-236), which has a mean radial velocity of -210 km/sec. The former group of filaments has, as expected, a lower Hα/[NII] ratio (about 0.3) than does the latter group (about 0.5).

The heat energy accruing to the nebula from such collisions will be (if the interstellar medium has a density of 0.1/cc, the nebula expands outward at a rate of 1500 km sec, and the conversion to heat energy is complete) about 3×10^{37} ergs/sec. This heat energy will be gained at the expense of the kinetic energy of the expansion which is, in turn, maintained at the expense of the magnetic field energy and the energy of the relativistic particles (see section V.D).

The total energy radiated in all emission lines from 3700 Å to 5100 Å is about 8×10^{34} ergs/sec (Woltjer, 1958). The red lines of H, [NII], [SII], and [OI] radiate about an equal amount, raising the total to 2×10^{35} ergs/sec in the optical region. The energy radiated in the ultraviolet will be, at most, about the same as the optical radiation, since (for a temperature of 10,000°) the number of particles sufficiently energetic to excite a line at λ1000 is down by a factor of 50 from the number available at λ3700. The cooling rate due to the

collisional excitation of the fine structure levels of O, Ne, N, and C has been calculated as a function of electron temperature by Osterbrock (1965). If the filamentary part of the Crab Nebula has an average electron density of 10^3 and fills a volume of 2×10^{53} cm^3, then the energy lost in infrared line radiation due to this process will be about 10^{36} ergs/sec at a temperature of $10,000^{\circ}$ and twice that at $15,000^{\circ}$. The energy imparted to the nebula by collision with the interstellar medium is, therefore, ample to maintain the observed rates of line radiation and the temperatures implied by them, which the synchrotron radiation alone could not do.

On the other hand, ultraviolet synchrotron radiation with a spectral index of 1.5 is just right to maintain the observed degree of ionization, which collisions alone cannot do at electron temperatures acceptable for the Crab Nebula.

G. Possible Future Studies

Several of the uncertainties discussed above could probably be cleared up by further work. It may not be possible to improve the proper motion measurements very much. Although direct plates taken in the future will provide longer and longer base lines, the increasing brightness of the night sky around Mt. Wilson and Mt. Palomar and the increasingly heavy demands on telescope time are rapidly reducing the chances of obtaining plates of quality comparable to the early ones. Motions for additional filaments can readily be obtained from the present plates.

New spectra are much more likely to be useful. Additional radial velocities, particularly of filaments near the edges of the nebula, could both settle the question of the existence of real deviations from uniform expansion and greatly improve our knowledge of the three dimensional distribution of matter in the Crab Nebula.

Absolute photometry of the line spectrum (obtained photoelectrically or from spectra with photoelectric standards) would be particularly valuable. Good determinations of four line ratios at a number of points in the nebula should go far toward removing the remaining uncertainties of temperature and energy balance in the filaments.

Three of these four ratios, [OII] $\lambda 3726/\lambda 3729$ (which is primarily sensitive to density), [OIII] $\lambda 4363/\lambda 5000$ (which is primarily sensitive to electron temperature), and [OII]/[OIII] (which is primarily sensitive to ionization) are relatively easily determined. The ratio $H\alpha$ $H\beta$, because of the large difference in wavelength between the two lines, is rather more difficult to obtain. It should, however, indicate definitely whether the excitation is primarily radiative or collisional at various points in the nebula. This question is distinct from the one of whether, as seems to be the case, the nebula derives a significant amount of heat energy from interactions with the interstellar medium.

The amount of energy radiated by the filaments could be better established by measurements of absolute line intensities for the nebula as a whole, such as that found by O'Dell (1962) for the lines

N1 + N2 + Hβ.

The two most interesting regions of the nebula for further work seem to be the center and the extreme edges. A precise position for the small diameter, low frequency radio source is important for several reasons. It is not likely that there would be two separate unusual points in the Crab Nebula, hence, if there is any star-like remnant of the supernova event, it is surely associated with the low frequency source. Thus, if the small radio source should prove not to fall near any of the stars at the center of the nebula, it could safely be concluded that none of the stars is physically related to the nebula. In addition, the position of the low frequency radio source would be a good choice for the present center of mass of the object to be used in finding its overall proper motion. If the source should be near the expansion center, then the space motion found for the Crab Nebula would no longer be unusual. The position of the small radio source is presumably also the position of the point source of activity in the continuum emission suggested by Scargle (1968).

A good spectrum of the south preceding component of the central double star, or of any other star that may prove to lie close to the small diameter radio source, would be interesting. A reasonably normal spectrum would be grounds for concluding that the star is probably not related to the nebula, while an unusual spectrum would tend to support the connection. In the latter case, the radial velocity of the star could help to establish the space motion of both objects.

Münch (private communication) has considered the possibility of using an elliptical diaphragm to obtain a spectrum of the entire outer edge of the nebula. Such a spectrum would give both the average radial velocity of the nebula and the dispersion around that velocity, which will represent the deviations from uniform expansion. This dispersion in velocity near the edges will be much smaller than that for the nebula as a whole. As a result, weak lines (such as [FeII]) which cannot be seen in an integrated spectrum of the nebula should be detectable, since the lines will be much narrower.

Line intensity ratios from such a spectrum would also be most interesting. If, as suggested in section V.F, the Crab Nebula gains considerable heat energy from collision with the interstellar medium, it should have a thin outer shell of very high ionization and electron temperature. A spectrum of the faint outer region should, therefore, show a higher average temperature than is found for the stronger features whose temperatures are discussed above. It is possible that evidence for extremely high temperatures in a small part of the nebula could also be found from a spectrum of the outer edges. Shklovskii (1962) suggested that temperatures as high as 10^6 or $10^{7\,o}$ ought to occur immediately behind the shock front on the outside of an expanding supernova remnant. Shcheglov (1968) has reported the detection of a coronal line, Fe X λ6374, in a portion of the Cygnus Loop, indicating temperatures of that order. Similar lines may be emitted from an outer shell of the Crab Nebula and might be visible on such a spectrum of the edge of the nebula.

Finally, something ought to be done with all this data as well as that presented by Scargle (1968) and the various recent X-ray, gamma-ray, and radio observations. In particular, it should be possible to construct a model for the Crab Nebula that will explain the observed motions of the filamentary and amorphous components of the nebula, their interaction with the interstellar medium, and the distribution of relativistic and thermal gases, radiation, and energy in the present nebula as well as its earlier stages.

TABLE III

PROPER MOTIONS OF FILAMENTS SHOWN IN FIG. 1

Filament	x Arcsec	y Arcsec	μ_x "/yr	μ_y "/yr	μ_r "/yr	E_μ %	α Deg.	σ_α Deg.
1	+140.1	- 59.4	+.157	-.052	.166	2.1	108.2	1.0
2	+133.5	- 59.9	+.156	-.030	.159	2.1	100.8	1.8
3	+125.5	- 65.5	+.154	-.072	.170	4.9	115.2	0.5
4	+132.3	- 41.4	+.145	-.026	.148	0.5	100.2	4.5
5	+ 22.6	-112.4	+.018	-.123	.124	13.5	171.5	0.9
6	+ 96.4	+ 38.3	+.113	+.062	.130	6.8	51.1	0.8
7	+ 82.6	- 90.5	+.086	-.115	.146	3.5	142.7	7.8
8	+ 19.5	- 75.5	+.008	-.077	.078	11.1	174.1	2.8
9	- 31.2	- 85.5	-.018	-.083	.086	14.1	192.5	2.0
10	- 35.1	- 89.3	-.021	-.082	.086	19.4	193.0	7.2
11	- 84.1	- 49.4	-.106	-.051	.119	6.3	244.1	5.0
12	- 97.6	- 53.5	-.132	-.058	.144	2.7	246.2	1.9
13	- 94.8	- 47.9	-.132	-.042	.138	5.2	252.4	1.6
14	- 70.4	+ 93.4	-.105	+.122	.164	3.2	319.5	9.5

TABLE III (Continued)

Filament	x Arcsec	y Arcsec	μ_x "/yr	μ_y "/yr	μ_r "/yr	E_μ %	α Deg.	σ_α Deg.
15	- 20.8	+129.7	-.009	+.178	.178	3.0	357.1	2.1
16	-110.8	+ 94.2	-.143	+.131	.194	2.0	312.4	1.7
17	-117.0	+ 89.0	-.158	+.142	.212	0.6	311.9	2.4
18	+110.9	+ 9.7	+.122	+.028	.126	6.0	75.7	2.0
19	+ 50.5	-110.4	+.057	-.114	.128	1.4	153.3	6.4
20	-106.2	+ 32.3	-.135	+.050	.145	4.2	290.6	3.1
21	+ 49.2	+119.3	+.036	+.155	.159	0.2	12.9	1.9
22	+ 48.8	+122.1	+.045	+.155	.162	8.1	16.3	1.2
23	+ 68.3	+ 80.5	+.069	+.125	.143	4.2	28.6	5.6
24	- 68.3	+109.3	-.089	+.130	.157	2.1	325.4	2.0
25	- 62.5	- 90.6	-.085	-.090	.124	0.0	223.5	0.0
26	- 85.8	-100.1	-.119	-.111	.163	0.4	226.9	1.7
27	-130.6	+ 46.3	-.174	+.056	.183	2.6	287.7	1.8
28	-108.3	+ 60.6	-.146	+.087	.170	6.3	300.9	2.6
29	-104.0	- 1.5	-.128	-.004	.128	21.3	267.2	4.0

TABLE III (Continued)

Filament	x Arcsec	y Arcsec	μ_x "/yr	μ_y "/yr	μ_r "/yr	E_μ %	α Deg.	σ_α Deg.
30	- 95.9	- 24.8	-.132	-.010	.133	7.6	265.6	0.1
31	- 84.5	- 28.2	-.119	-.012	.121	4.6	264.1	6.8
32	+ 42.0	- 77.3	+.054	-.080	.096	4.5	145.8	6.0
33	+ 87.4	+ 67.3	+.118	+.115	.165	2.8	45.6	0.8
34	+ 12.0	+110.7	+.013	+.150	.151	1.0	4.9	3.0
35	- 7.0	+120.7	-.022	+.157	.159	15.0	352.7	4.2
36	+ 86.3	- 15.2	+.084	-.002	.084	17.2	92.0	2.8
37	- 85.8	+123.3	-.100	+.162	.191	7.6	327.9	3.2
38	+116.0	+ 8.1	+.166	+.027	.169	13.6	80.9	0.1
39	+126.0	+ 4.8	+.136	+.021	.133	8.1	80.7	1.6
40	+131.0	- 8.7	+.144	+.020	.146	4.3	82.3	6.8
41	+155.0	- 25.4	+.126	-.051	.136	29.3	113.7	5.1
42	+139.5	- 40.4	+.134	-.030	.138	7.5	102.7	2.1
43	+103.0	- 77.0	+.126	-.084	.154	6.3	124.4	9.1
44	+ 91.0	- 79.4	+.122	-.087	.150	1.1	125.3	1.3

TABLE III (Continued)

Filament	x Arcsec	y Arcsec	μ_x "/yr	μ_y "/yr	μ_r "/yr	E_μ %	α Deg.	σ_α Deg.
45	+ 42.4	-133.0	+.025	-.148	.150	1.4	170.3	0.5
46	+ 18.7	-109.1	+.009	-.132	.132	8.2	176.0	0.8
47	- 10.1	- 80.1	-.017	-.083	.086	10.8	192.8	9.4
48	- 20.8	- 86.6	-.048	-.092	.104	1.2	207.4	4.3
49	- 35.1	-100.6	-.049	-.114	.124	13.2	203.1	1.6
50	- 64.7	- 97.5	-.079	-.106	.132	13.4	216.4	3.0
51	- 81.0	- 84.7	-.095	-.082	.126	19.0	230.4	5.8
52	-105.6	- 71.0	-.136	-.098	.169	0.5	234.1	5.1
53	- 86.6	- 70.8	-.113	-.072	.134	0.8	237.4	2.8
54	-105.0	- 59.8	-.138	-.066	.154	3.8	243.9	1.4
55	-116.9	- 28.2	-.140	-.026	.143	5.4	259.2	1.2
56	-118.7	- 5.7	-.138	-.028	.141	1.7	258.3	3.6
57	-132.9	+ 1.7	-.150	-.002	.150	17.6	269.2	1.2
58	-141.0	+ 11.3	-.212	+.020	.214	11.2	275.0	5.0
59	-145.0	+ 34.7	-.221	+.044	.225	5.3	281.1	0.1

TABLE III (Continued)

Filament	x Arcsec	y Arcsec	μ_x "/yr	μ_y "/yr	μ_r "/yr	E_μ %	α Deg.	σ_α Deg.
60	-105.6	+ 70.7	-.153	+.085	.176	1.8	299.1	5.1
61	-144.6	+ 76.4	-.177	+.096	.202	11.1	298.4	0.9
62	-104.2	+ 91.0	-.132	+.132	.186	0.2	314.9	1.5
63	- 93.4	+109.3	-.118	+.139	.183	2.0	319.6	1.6
64	- 60.2	+112.2	-.080	+.147	.168	3.8	331.2	1.1
65	- 60.9	+122.4	-.056	+.158	.168	4.9	340.6	4.2
66	- 15.0	+ 98.2	-.032	+.118	.124	4.8	345.6	8.1
67	- 5.5	+105.7	-.019	+.138	.139	1.4	352.4	4.0
68	+ 19.5	+110.6	+.014	+.141	.142	3.0	6.0	3.0
69	+ 37.1	+ 93.2	+.038	+.137	.143	7.3	14.8	6.4
70	+ 49.8	+ 87.4	+.052	+.101	.115	15.3	28.1	4.5
71	+ 72.8	+ 76.2	+.061	+.105	.122	18.2	29.0	5.0
72	+ 82.9	+ 84.4	+.103	+.139	.173	6.6	36.7	0.9
73	+101.9	+ 69.0	+.115	+.084	.143	2.1	54.2	5.0
74	+ 99.2	+ 50.3	+.110	+.073	.133	2.9	56.6	5.3

TABLE III (Continued)

Filament	x Arcsec	y Arcsec	μ_x "/yr	μ_y "/yr	μ_r "/yr	E_μ %	α Deg.	σ_α Deg.
75	+ 96.7	+ 29.1	+.112	+.043	.120	8.8	68.4	7.4
76	+ 45.1	- 29.6	+.050	-.032	.063	21.8	127.0	19.0
77	+ 62.3	- 24.2	+.062	-.009	.063	24.0	98.4	0.2
78	+ 71.7	- 22.4	+.076	-.003	.077	7.6	92.6	5.2
79	+ 54.8	- 47.6	+.041	-.042	.059	20.4	134.3	6.1
80	+ 74.4	- 38.1	+.062	-.013	.063	4.0	102.4	4.6
81	+103.5	- 33.0	+.087	-.016	.088	8.4	100.2	2.1
82	+ 30.8	- 8.9	+.032	-.001	.033	2.2	91.3	11.5
83	+ 44.7	- 2.0	+.046	+.016	.049	7.4	70.7	4.5
84	+ 62.5	+ 5.1	+.071	+.020	.074	3.4	74.4	0.3
85	+ 44.0	+ 15.5	+.047	+.037	.060	11.8	51.8	2.5
86	+ 51.8	+ 26.6	+.059	+.039	.071	24.4	56.8	1.0
87	+ 63.8	+ 41.7	+.070	+.059	.094	20.3	46.9	13.5
88	+ 27.1	+ 37.3	+.024	+.059	.064	1.2	21.7	0.5
89	+ 46.9	+ 52.3	+.054	+.088	.103	13.0	31.2	0.4

TABLE III (Continued)

Filament	x Arcsec	y Arcsec	μ_x "/yr	μ_y "/yr	μ_r "/yr	E_μ %	α Deg.	σ_α Deg.
90	+ 39.6	+ 71.2	+.035	+.087	.094	2.6	22.1	4.2
91	+ 20.0	+ 49.1	+.013	+.063	.065	12.2	12.3	6.8
92	+ 37.0	+ 59.7	+.045	+.091	.102	0.1	26.3	1.8
93	+ 4.5	+ 59.6	-.015	+.080	.082	3.2	342.0	2.0
94	+ 16.3	+ 79.9	+.013	+.102	.103	6.1	7.6	2.6
95	- 5.5	+ 88.4	-.005	+.119	.119	1.1	2.3	2.8
96	- 32.9	+ 66.9	-.039	+.096	.105	4.6	337.8	4.8
97	- 33.1	+ 84.4	-.044	+.104	.114	3.9	337.1	1.9
98	- 50.2	+ 97.8	-.053	+.138	.148	0.1	339.1	2.5
99	- 51.0	+ 66.0	-.066	+.081	.105	6.6	320.7	0.9
100	- 72.9	+ 80.1	-.112	+.111	.158	2.5	315.0	1.2
101	- 76.2	+ 54.1	-.112	+.088	.143	3.2	308.0	3.5
102	- 85.5	+ 23.2	-.117	+.033	.122	1.4	285.6	1.4
103	- 64.0	+ 19.9	-.079	+.020	.083	13.2	282.6	10.1
104	- 69.1	+ 38.8	-.098	+.036	.105	2.9	290.1	4.5

TABLE III (Continued)

Filament	x Arcsec	y Arcsec	μ_x "/yr	μ_y "/yr	μ_r "/yr	E_μ %	α Deg.	σ_α Deg.
105	- 50.6	+ 33.1	-.064	+.047	.080	33.2	303.2	8.8
106	- 32.2	+ 47.9	-.043	+.089	.101	10.4	333.1	12.2
107	- 23.2	+ 20.0	-.040	+.023	.053	22.7	299.8	21.9
108	- 85.8	- 0.8	-.116	+.003	.116	1.2	271.6	1.6
109	- 57.3	- 0.5	-.080	-.001	.080	0.8	269.3	2.1
110	- 20.1	- 23.0	-.042	-.013	.045	56.6	249.9	5.5
111	- 64.1	- 19.3	-.073	-.012	.074	0.8	260.9	1.5
112	- 59.0	- 36.9	-.098	-.007	.102	5.2	264.8	15.6
113	- 61.4	- 59.1	-.093	-.053	.108	3.0	240.7	1.6
114	- 42.6	- 45.9	-.045	-.040	.060	1.6	228.5	3.8
115	- 30.1	- 57.4	-.068	-.068	.097	3.4	224.9	5.3
116	- 9.2	- 57.5	-.015	-.069	.071	1.3	191.8	8.1
117	+ 18.7	- 43.5	-.004	-.039	.039	56.6	183.1	3.8
118	+ 84.5	- 64.0	+.106	-.056	.120	3.8	117.7	0.3
119	+156.0	- 56.4	+.172	-.062	.183	0.8	109.6	1.6

TABLE III (Continued)

Filament	x Arcsec	y Arcsec	μ_x "/yr	μ_y "/yr	μ_r "/yr	E_μ %	α Deg.	σ_α Deg.
120	+146.8	- 4.6	+.127	+.017	.128	62.2	82.4	9.9
121	+120.5	+ 58.9	+.156	+.086	.180	4.8	60.7	8.6
122	+ 24.7	+134.1	+.015	+.073	.174	3.1	4.8	4.8
123	- 1.6	+133.3	+.003	+.160	.161	2.8	1.0	7.0
124	- 58.0	+143.6	-.070	+.184	.198	2.2	339.3	5.6
125	-110.0	+125.2	-.148	+.158	.217	1.1	317.0	1.2
126	-131.8	+ 90.2	-.160	+.104	.191	8.8	303.3	1.2
127	-151.8	+ 54.8	-.202	+.073	.215	14.8	290.3	3.6
128	- 24.1	-110.6	-.035	-.120	.125	1.8	196.3	1.8
129	+ 63.0	-141.4	+.038	-.156	.161	10.8	166.0	3.4
130	+112.8	-111.9	+.141	-.137	.198	4.9	134.5	5.9
131	+131.5	- 83.1	+.162	-.112	.167	2.7	125.7	2.1
132	- 32.9	- 15.9	-.052	-.015	.054	5.8	253.9	3.6

TABLE IV

PROPER MOTIONS AND RADIAL VELOCITIES OF FILAMENTS SHOWN IN FIG. 3

Filament	x Arcsec	y Arcsec	μ_x "/yr	μ_y "/yr	V_r km/sec	σ_v km/sec
133	- 31.1	+ 89.8	-.035	+.105	+ 56	7
134	- 46.9	+ 98.4	-.066	+.125	+130	14
135	- 37.1	+ 94.6	-.051	+.126	+113	16
136	- 55.7	+100.9	-.077	+.123	+125	-
137	- 7.1	+ 65.4	-.018	+.095	-311	11
138	- 11.7	+ 61.3	-.019	+.081	-527	4
139	- 19.3	+ 54.6	-.030	+.065	-662	6
140	- 31.4	+ 35.8	-.039	+.042	+1382	-
141	- 23.6	+ 37.1	-.027	+.055	-719	20
142	- 45.9	+ 25.6	-.064	+.026	-932	20
143	- 45.3	+ 20.3	-.062	+.033	-918	-
144	- 66.4	+ 6.5	-.098	+.012	-439	24
145	+ 1.4	+ 49.4	-.012	+.062	+874	28
146	+ 86.8	+ 44.3	+.088	+.063	- 84	-

TABLE IV (Continued)

Filament	x Arcsec	y Arcsec	μ_x "/yr	μ_y "/yr	V_r km/sec	σ_v km/sec
147	+ 94.1	+ 35.9	+.110	+.054	-274	28
148	+ 97.3	+ 28.2	+.106	+.046	-234	-
149	+ 94.1	+ 13.7	+.102	+.030	-601	-
150	+ 95.8	+ 11.3	+.095	+.064	-672	-
151	+103.5	- 32.5	+.096	-.025	+844	33
152	+ 89.0	+ 40.8	+.114	+.055	-808	5
153	+ 96.2	+ 38.1	+.113	+.059	+ 18	1
154	+ 99.3	+ 35.9	+.117	+.060	+498	36
155	+101.9	+ 30.2	+.127	+.054	+ 39	5
156	+105.9	+ 19.9	+.125	+.042	-550	6
157	- 19.2	- 0.3	-.032	+.014	-698	46
158	- 9.4	- 0.9	-.013	-.001	+ 89	0.1
159	- 2.9	- 0.4	-.003	+.000	-162	50
160	+ 4.6	+ 0.8	-.007	+.002	-369	16
161	+ 57.2	- 1.2	+.054	+.009	+950	13

TABLE IV (Continued)

Filament	x Arcsec	y Arcsec	μ_x "/yr	μ_y "/yr	V_r km/sec	σ_v km/sec
162	+ 26.7	+ 92.1	+.026	+.117	+631	102
163	+ 12.3	+ 92.1	+.013	+.117	-304	30
164	- 3.6	+ 91.7	-.005	+.122	+130	42
165	- 13.8	+ 89.5	-.027	+.133	+102	7
166	- 28.0	+ 88.4	-.038	+.104	+119	25
167	- 23.0	+ 88.6	-.032	+.128	-455	8
168	- 54.1	+ 88.3	-.075	+.118	-350	-
169	- 65.1	+ 84.4	-.093	+.110	-962	-
170	+ 55.0	+ 78.0	+.047	+.095	-145	34
171	+ 48.5	+ 47.5	+.043	+.067	+340	6
172	+ 41.4	+ 13.1	+.032	+.013	+484	3
173	+ 43.1	+ 11.3	+.046	+.013	+548	24
174	+ 44.6	- 2.0	+.042	+.010	-293	-
175	+ 37.8	+ 2.7	+.044	+.020	-882	-
176	+ 33.7	- 31.3	+.037	-.012	+683	13

TABLE IV (Continued)

Filament	x Arcsec	y Arcsec	μ_x "/yr	μ_y "/yr	V_r km/sec	σ_v km/sec
177	+ 30.2	- 54.8	+.020	-.057	+439	9
178	+ 30.2	- 71.0	+.031	-.102	+ 80	16
179	+ 24.4	- 78.4	+.018	-.107	+557	32
180	-126.5	- 94.6	-.153	-.150	-879	2
181	-107.0	-100.9	-.122	-.135	-732	8
182	- 86.6	-100.6	-.098	-.122	-217	50
183	- 76.3	+ 0.0	-.102	+.003	-376	14
184	- 68.7	- 0.6	-.101	-.006	-313	14
185	- 87.1	+ 11.1	-.119	+.010	-198	10
186	- 93.2	+ 17.5	-.126	+.022	-142	14
187	- 85.9	- 0.9	-.121	-.002	-698	-
188	-106.4	+ 22.6	-.126	+.033	-798	-
189	-112.9	+ 25.5	-.162	+.033	-960	-
190	-121.0	+ 29.9	-.148	+.046	+716	9
191	-138.7	+ 40.7	-.185	+.060	+444	-

TABLE IV (Continued)

Filament	x Arcsec	y Arcsec	μ_x "/yr	μ_y "/yr	V_r km/sec	σ_v km/sec
192	-147.9	+ 49.6	-.188	+.063	+356	-
193	+ 26.4	- 61.3	+.022	-.064	+463	19
194	- 23.6	- 30.0	-.039	-.023	+797	19
195	- 29.6	- 22.6	-.051	-.018	+682	8
196	- 31.7	- 22.1	-.064	-.013	+544	8
197	- 27.8	- 29.3	-.051	-.028	-665	1
198	- 35.6	- 27.8	-.064	-.018	-544	13
199	- 38.2	- 26.1	-.063	-.026	-432	4
200	- 47.5	- 18.3	-.082	-.017	-408	7
201	- 65.4	- 9.0	-.095	-.000	-403	16
202	- 79.3	+ 1.4	-.095	+.010	-316	5
203	- 31.9	- 29.5	-.053	-.021	-596	18
204	- 35.7	- 20.1	-.058	-.015	-487	17
205	- 83.4	+ 6.6	-.097	+.013	-232	13
206	+ 52.6	+ 6.6	+.051	+.023	+404	24

TABLE IV (Continued)

Filament	x Arcsec	y Arcsec	μ_x "/yr	μ_y "/yr	V_r km/sec	σ_v km/sec
207	+ 30.4	- 0.7	+.022	+.014	-777	18
208	+ 17.9	- 4.2	+.008	+.016	-733	7
209	+ 25.5	- 7.9	+.018	+.010	+682	13
210	- 84.0	- 49.6	-.114	-.049	+210	36
211	+ 8.0	+ 58.0	+.000	+.084	+598	16
212	+ 15.6	+ 63.7	+.006	+.085	+871	-
213	+ 16.9	+ 70.1	+.005	+.095	-738	8
214	+ 18.3	+ 62.3	+.011	+.084	-823	10
215	+ 9.2	+ 62.2	+.002	+.086	-889	11
216	+ 5.7	+ 54.5	+.011	+.086	+782	12
217	+ 7.4	+ 46.2	-.006	+.054	-1122	-
218	- 10.7	+ 25.5	-.029	+.044	+1299	-
219	- 11.9	+ 19.6	-.027	+.037	+1140	15
220	- 21.1	+ 7.8	-.033	+.009	-1482	44
221	- 28.1	- 3.2	-.038	-.001	-1385	21

TABLE IV (Continued)

Filament	x Arcsec	y Arcsec	μ_x "/yr	μ_y "/yr	V_r km/sec	σ_v km/sec
222	- 30.7	+ 0.7	-.043	+.010	+1086	37
223	- 28.2	- 8.3	-.048	+.010	-919	10
224	- 30.0	- 12.6	-.055	-.001	-451	-
225	- 37.0	- 8.4	-.061	+.007	+920	27
226	- 36.8	- 12.0	-.065	+.004	-566	22
227	- 38.4	- 23.7	-.070	+.013	-448	18
228	+ 62.3	+ 75.9	+.060	+.111	-179	11
229	+ 53.9	+ 68.4	+.052	+.079	+378	-
230	+ 45.8	+ 67.4	+.037	+.098	+522	-
231	+ 43.3	+ 62.3	+.036	+.073	+550	-
232	+ 38.0	+ 62.2	+.022	+.078	+500	3
233	+ 49.4	+ 72.9	+.048	+.097	- 62	-
234	+ 44.6	+ 70.2	+.042	+.099	-155	21
235	+ 40.0	+ 68.1	+.032	+.091	-297	36
236	+ 35.8	+ 69.4	+.017	+.095	-327	30

TABLE IV (Continued)

Filament	x Arcsec	y Arcsec	μ_x "/yr	μ_y "/yr	V_r km/sec	σ_v km/sec
237	+ 31.8	+ 60.9	+.022	+.082	-536	25
238	+ 21.8	+ 63.5	+.001	+.081	-561	29
239	- 5.3	+ 50.1	-.010	+.071	+1313	-
240	- 9.6	+ 50.7	-.015	+.071	+1144	15
241	- 25.3	+ 43.1	-.034	+.064	+982	30
242	- 30.8	+ 45.2	-.048	+.063	+850	16
243	- 12.8	+ 53.6	-.029	+.070	-336	10
244	- 27.9	+ 43.6	-.031	+.064	-591	12
245	- 32.3	+ 48.1	-.042	+.071	-749	5
246	- 36.7	+ 41.1	-.067	+.063	+1647	-
247	- 62.2	+ 35.1	-.101	+.047	+1470	-
248	- 44.4	+ 44.0	-.065	+.055	-1026	-
249	- 61.5	+ 39.4	-.083	+.052	-948	2
250	- 68.9	+ 33.6	-.095	+.043	-980	-
251	- 78.8	+ 33.4	-.106	+.047	+964	0.4

TABLE IV (Continued)

Filament	x Arcsec	y Arcsec	μ_x "/yr	μ_y "/yr	V_r km/sec	σ_v km/sec
252	- 90.1	+ 29.5	-.123	+.036	+1135	4
253	+ 39.5	+ 71.1	+.043	+.098	-379	85
254	+ 32.6	+ 66.9	+.023	+.094	-502	20
255	+ 43.5	+ 48.6	+.049	+.068	+264	12
256	+ 35.4	+ 55.5	+.041	+.073	-365	5
257	+ 11.9	+ 69.7	+.010	+.091	+473	12
258	+ 3.7	+ 75.3	-.018	+.091	+199	13
259	- 16.2	+ 80.9	-.023	+.097	-609	26

REFERENCES

Aller, L. H. 1961, Abundance of the Elements, (New York: Interscience Publishers, Inc.), pp. 179 ff.

Baade, W. 1942, Ap. J., 96, 109.

Binnendijk, L. 1943, B.A.N., 10, 9.

Blaauw, A. 1961, B.A.N., 15, 265.

Bower, S., Byram, E.T., Chubb, T. A., and Friedman, H. 1964, Science, 146, 912.

Brosche, P. 1966, Zs.f.Ap., 64, 1.

Burbidge, G. R. 1958, Ap. J., 127, 48.

Burbidge, E. M. and Burbidge, G. R. 1962, Ap. J., 135, 694.

Clark, B. G., Radhakrishnan, V., and Wilson, R. W. 1962, Ap. J., 135, 151.

Collins, G. W., Daub, C. T., and O'Dell, C. R. 1961, Ap. J., 133, 471.

Delhaye, J. 1966, Galactic Structure, ed. A. Blaauw and M. Schmidt (Chicago: University of Chicago Press), p. 74.

Deutsch, A. N. and Lavdovsky, V. V. 1940, Poulkovo Obs. Circ., 30, 21.

Duncan, J. C. 1921, Proc. Nat. Acad. Sci., 7, 179.

Duncan, J. C. 1939, Ap. J., 89, 482.

Duyvendak, J. J. L. 1942, P.A.S.P., 54, 91.

Felten, J. E. and Gould, R. J. 1966, Phys. Rev. Letters, 17, 401.

Garstang, R. H. 1951, M.N., 111, 114.

Ginzburg, V. L. and Syrovatskii, S. I. 1964, The Origin of Cosmic Rays, (New York: The Macmillan Company), p. 93.

Gower, J. F. R. 1967, Nature, 213, 1213.

Grader, R., Hill, R., Seward, F., and Toor, A. 1966, Science, 152, 1499.

Greenstein, J. L. 1968, private communication.

Greenstein, J. L. and Minkowski, R. 1953, Ap.J., 118, 1.

Greenstein, J. L. and Trimble, V. L. 1967, Ap.J., 149, 283.

Haymes, R. C., Ellis, D. V., Fishman, G. J., Kurfess, J. D., and Tucker, W. H. 1968, Ap.J., 151, L9.

Hubble, E. 1934, A.S.P. Leaflets, 1, 58 (No. 14, January 1928).

Johnson, F. M. and Townes, C. H. 1957, Ap.J., 126, 466.

Kamp, P. van de 1941, Annals of the New York Academy of Sciences, 42, 151.

_____ 1962, Astronomical Techniques, ed. Hiltner (Chicago: University of Chicago Press), p. 487.

Kraft, R. P. 1967, private communication.

Lampland, C. O. 1921, P.A.S.P., 33, 79.

Maanen, A. van 1928, Mt. W. Contr., No. 356.

Matveenko, L. I. and Sorochenko, R. L. 1968, Soviet Astronomy - A.J., 11, 557.

Mayall, N. U. 1937, P.A.S.P., 49, 101.

Minkowski, R. 1942a, Ap.J., 96, 306.

_____ 1942b, Ap.J., 96, 199.

_____ 1964, Annual Review of Astronomy and Astrophysics, Vol. 2, ed. L. Goldberg, A. Deutsch, and D. Layzer (Palo Alto: Annual Reviews, Inc.), p. 247.

_____ 1966, A.J., 71, 371.

Münch, G. 1958, Rev. Mod. Phys., 30, 1042.

Newton, I. S. 1686, Philosophiae Naturalis Principia Mathematica, (London: S. Pepys, Reg. Soc. Praeses), p. 12.

Oda, M., Bradt, H., Garmire, G., Spada, G., Sreekantan, B. V., Gursky, H., Giacconi, R., Gorenstein, P., and Waters, J.R. 1967, Ap.J., 148, L5.

O'Dell, C. R. 1962, Ap.J., 136, 809.

Oort, J. H. and Walraven, Th. 1956, B.A.N., 12, 285.

Orlova, O. N. 1966, Pub. Astr. Obs. Pulkova, 24, 115.

Osterbrock, D. E. 1957, P.A.S.P., 69, 227.

Osterbrock, D. E. 1965, Ap.J., 142, 1423.

Parker, R. A. R. 1964a, Ap.J., 139, 208.

_____ 1964b, Ap.J., 139, 493.

Pikelner, S. B. 1956, Astr. Zhur. SSSR, 33, 785.

Poveda, A. and Woltjer, L. 1968, Ap.J., (in press).

Rhijn, P. J. van 1965, Galactic Structure, ed. A. Blaauw and M. Schmidt, (Chicago: University of Chicago Press), p. 35.

Sanford, R. F. 1919, P.A.S.P., 31, 108.

Scargle, J. 1968, Thesis, California Institute of Technology.

Schmidt, M. 1957, B.A.N., 13, 247.

Schmidt, M. 1966, Galactic Structure, ed. A. Blaauw and M. Schmidt (Chicago: University of Chicago Press), p. 528.

Seaton, M. J. 1954, M.N., 114, 154.

Shcheglov, P. V. 1968, Soviet Astronomy - AJ, 11, 567.

Shklovskii, I. S. 1960, Cosmic Radio Waves, (Cambridge, Mass.: Harvard University Press), p. 287 ff.

Shklovskii, I. S. 1962, Soviet Astronomy - AJ., 6, 162.

_____ 1966, Soviet Astronomy - AJ, 10, 6.

Slipher, V. M. 1916, P.A.S.P., 28, 192.

Trimble, V. L. 1968, Thesis, California Institute of Technology.

Williams, R. E. 1967, Ap.J., 147, 556.

Woltjer, L. 1958, B.A.N., 14, 39.

FIGURE 1: Proper motions for 132 positions in the Crab Nebula as listed in Table III. The arrows represent the distance the filaments will move in about 270 years at their present rates. The center of the expansion is located at the point marked X. The stars used to align the plates for measurement and those nearest the center of the nebula are lettered. The photograph was taken through an H_α interference filter on the 200 inch telescope by Münch.

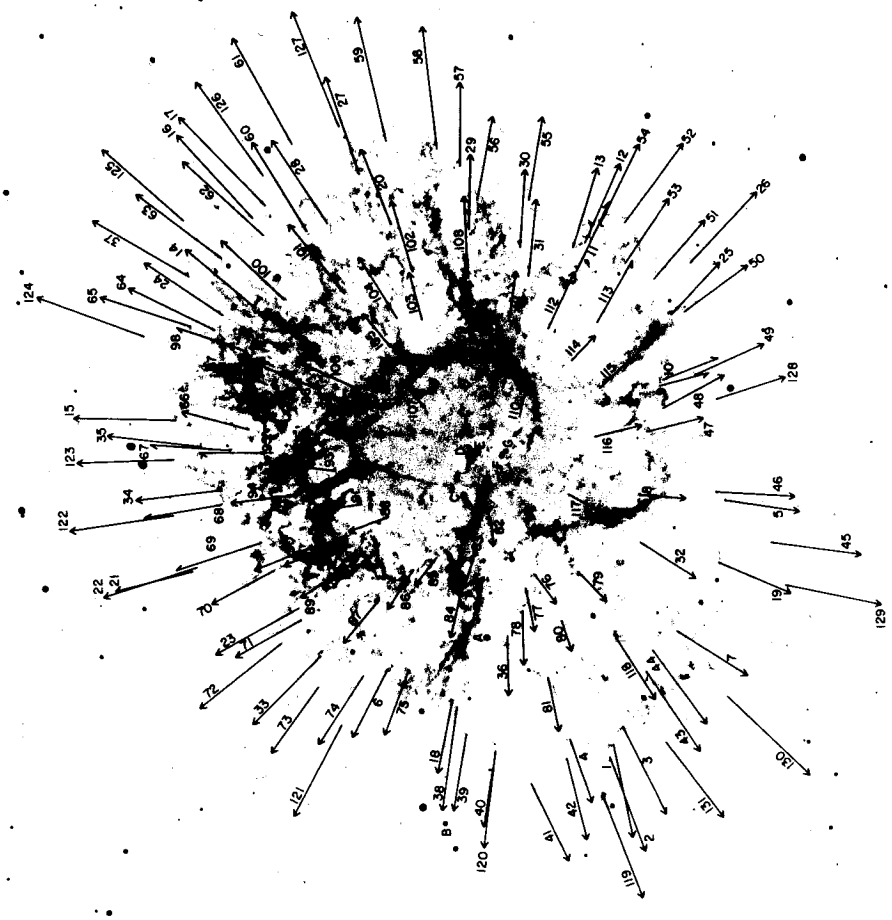

FIGURE 2: A typical spectrum of the Crab Nebula showing about 30 separate measurable features (some of which have been lost in the reproduction process). The two streaks perpendicular to the slit direction are stars separated by about 1'.5 in the plane of the sky. The lines of two or more features may be partially blended as, for example, at the points marked X.

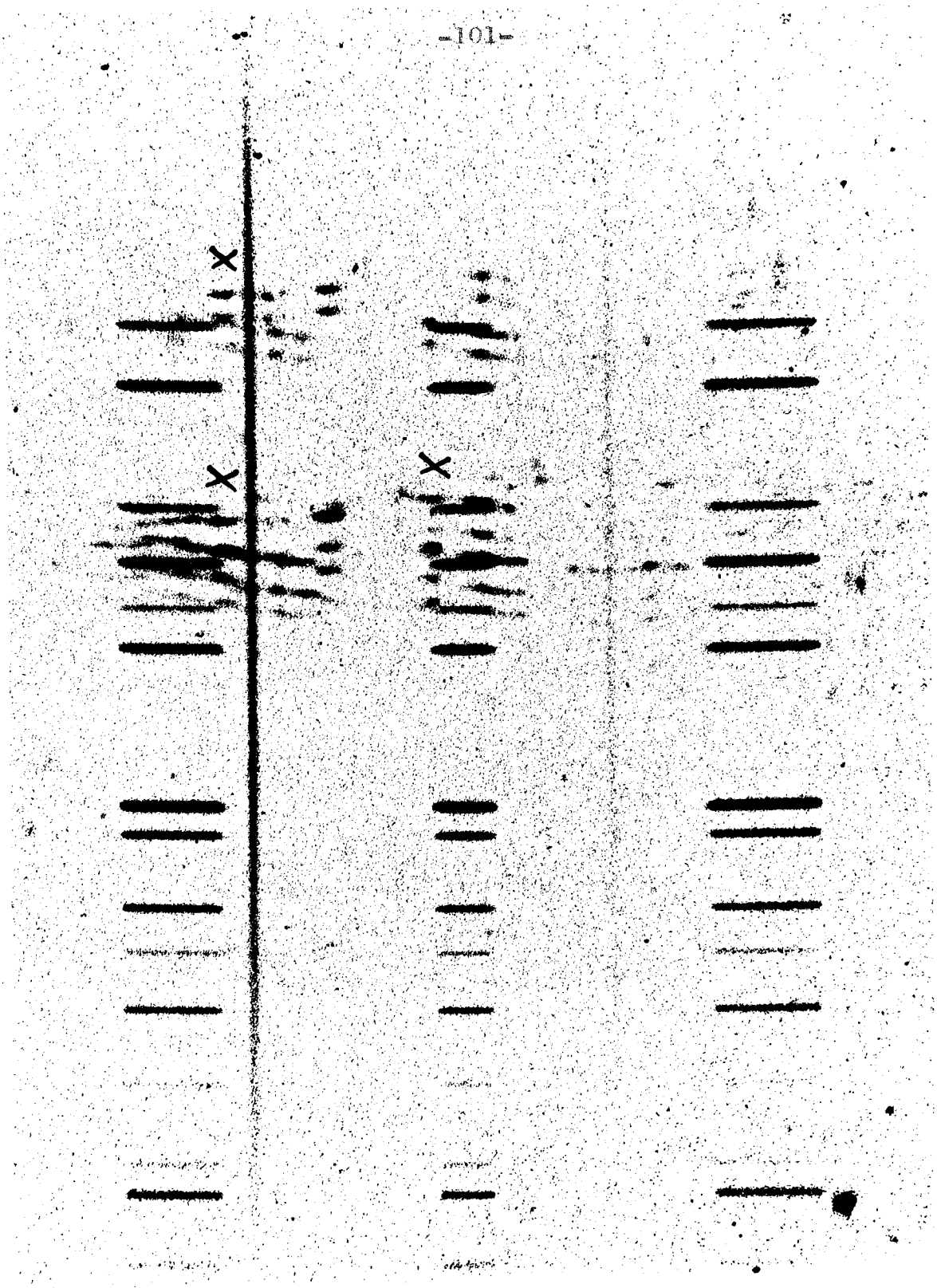

FIGURE 3: Proper motions for the 127 filaments of known radial velocities as listed in Table IV. The scale and orientation are about the same as in Figure 1, and X again marks the expansion center. The stars lettered in Fig. 1 are also shown.

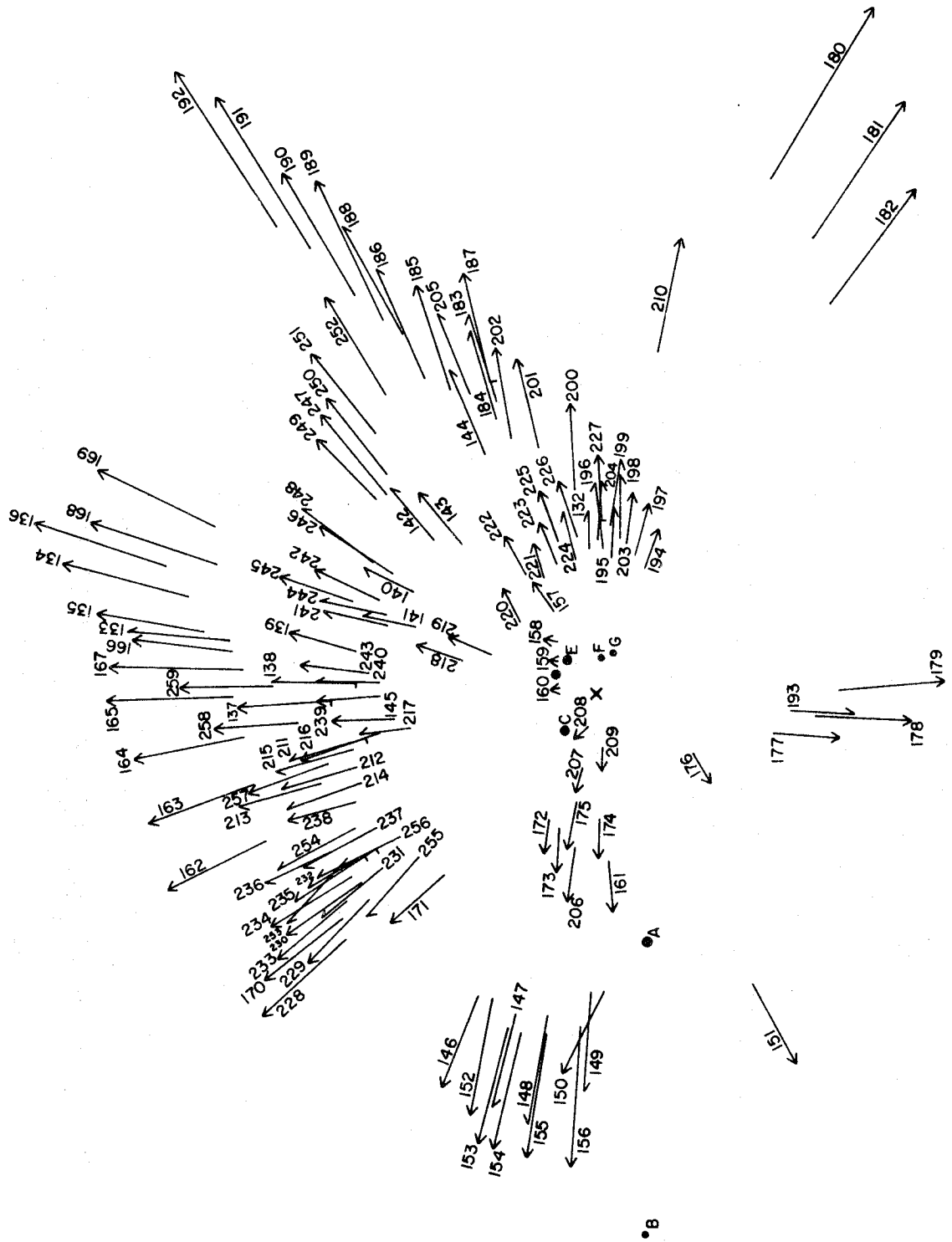
A
B
C
D
E
F
G
X
1
2
3
4
5
6
7
8
9
10
11
12
13
14
15
16
17
18
19
20
21
22
23
24
25
26
27
28
29
30
31
32
33
34
35
36
37
38
39
40
41
42
43
44
45
46
47
48
49
50
51
52
53
54
55
56
57
58
59
60
61
62
63
64
65
66
67
68
69
70
71
72
73
74
75
76
77
78
79
80
81
82
83
84
85
86
87
88
89
90
91
92
93
94
95
96
97
98
99
100
101
102
103
104
105
106
107
108
109
110
111
112
113
114
115
116
117
118
119
120
121
122
123
124
125
126
127
128
129
130
131
132
133
134
135
136
137
138
139
140
141
142
143
144
145
146
147
148
149
150
151
152
153
154
155
156
157
158
159
160
161
162
163
164
165
166
167
168
169
170
171
172
173
174
175
176
177
178
179
180
181
182
183
184
185
186
187
188
189
190
191
192
193
194
195
196
197
198
199
200
201
202
203
204
205
206
207
208
209
210
211
212
213
214
215
216
217
218
219
220
221
222
223
224
225
226
227
228
229
230
231
232
233
234
235
236
237
238
239
240
241
242
243
244
245
246
247
248
249
250
251
252
253
254
255
256
257
258
259

FIGURE 4: Central region of the Crab Nebula showing the expansion centers listed in Table V (C1 - C4 and their average) and the regions in which the filaments are concentrated at the time of best convergence. The present geometrical center of the nebula is shown as Δ . E1 and E2 are the 1054 positions of star E for proper motions of .019"/yr and .009"/yr respectively.

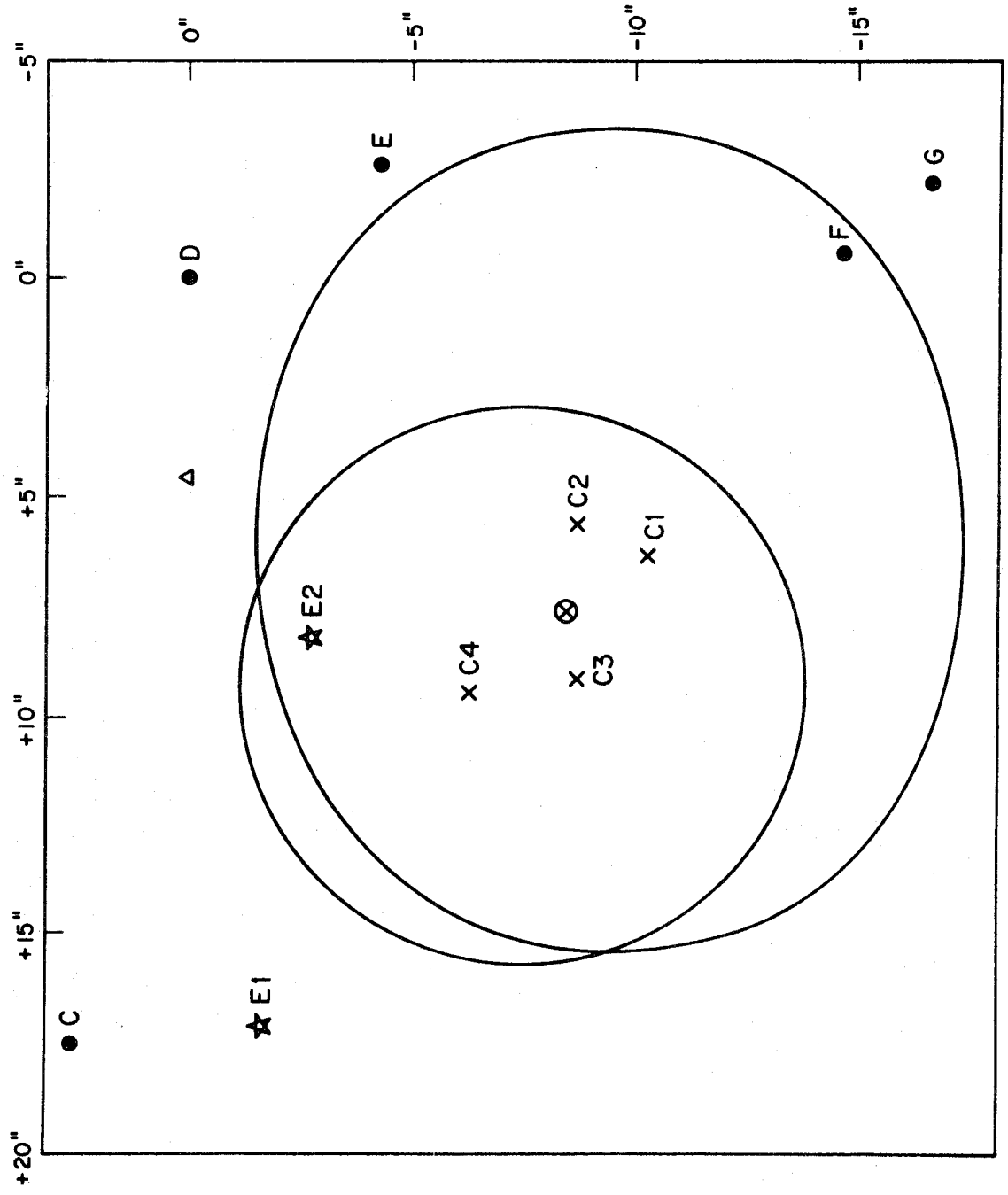
-5"
0"
+5"
+10"
+15"
+20"
0"
-5"
-10"
-15"
C
D
E
F
G
E1
E2
C1
C2
C3
C4

FIGURE 5: 1950 positions and motions in 270 years of the filaments of Table IV and Figure 3 projected onto the plane through the major axis of the nebula and the line of sight. The scale is the same as in Figures 1 and 3, and X is the expansion center. The coordinates are in arbitrary units centered at the position of star D in the plane of the sky.

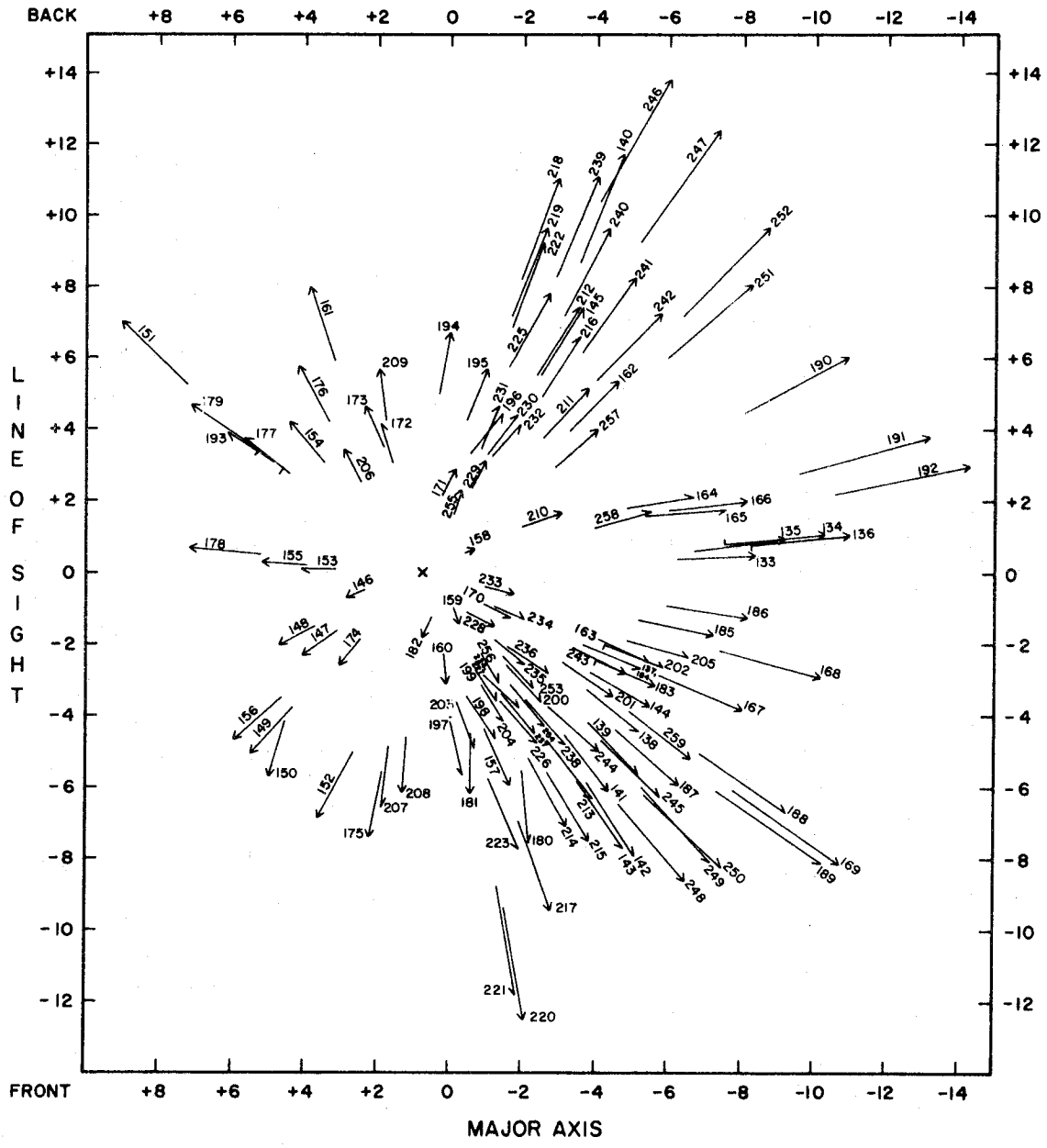
BACK
FRONT
LINE OF SIGHT
MAJOR AXIS
+8 +6 +4 +2 0 -2 -4 -6 -8 -10 -12 -14
+14 +12 +10 +8 +6 +4 +2 0 -2 -4 -6 -8 -10 -12

FIGURE 6: 1950 positions and motions in 270 years of the filaments of Table IV and Figure 3 projected onto the plane through the minor axis and the line of sight. Scale and coordinates as in Figure 5.

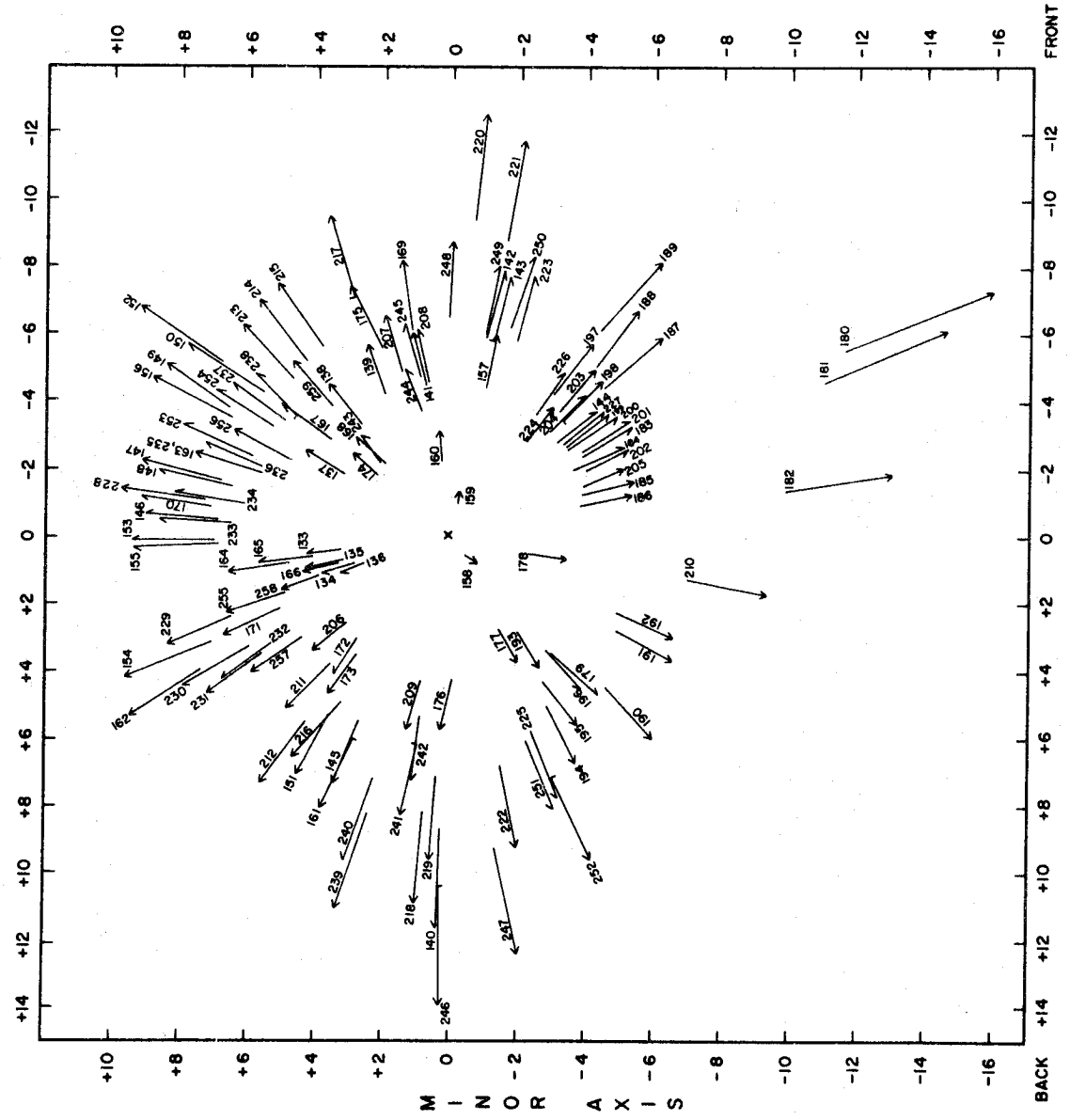
FRONT
BACK
LINE OF SIGHT
MINOR AXIS
+10
+8
+6
+4
+2
0
-2
-4
-6
-8
-10
-12
-14
-16
+12
+14

FIGURE 7: Histogram of the percentage errors, E_{μ}, of the lengths of the proper motion vectors as given in Table III.

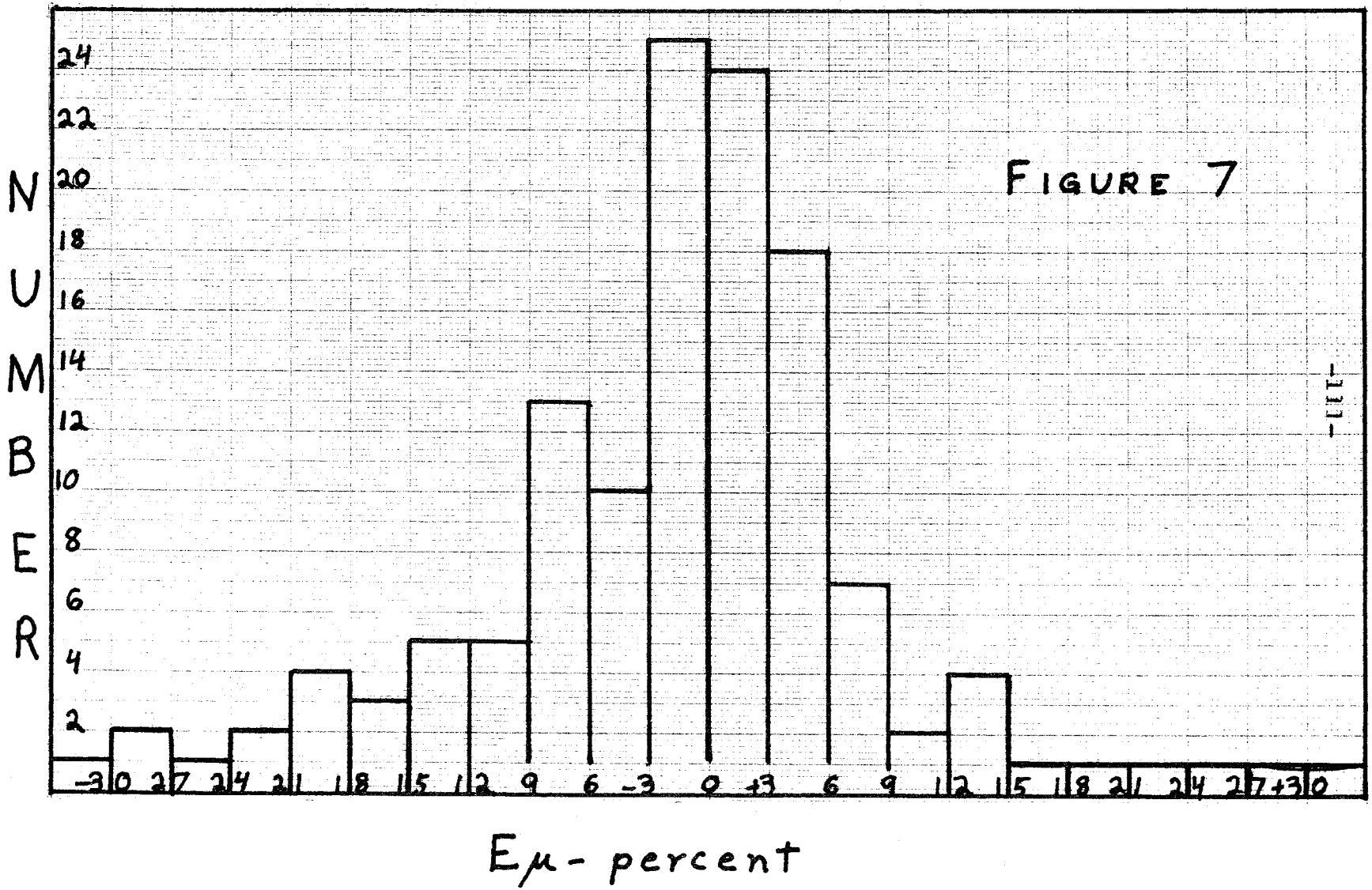
NUMBER
24
22
20
18
16
14
12
10
8
6
4
2
-3 0 2 7 2 4 2 1 1 8 1 5 1 2 9 6 -3 0 +3 6 9 1 2 1 5 1 8 2 1 2 4 2 7 +3 0
Eμ - percent

FIGURE 7

FIGURE 8: Histogram of the probable errors, σ_α, of the position angles of the proper motion vectors as given in Table III.

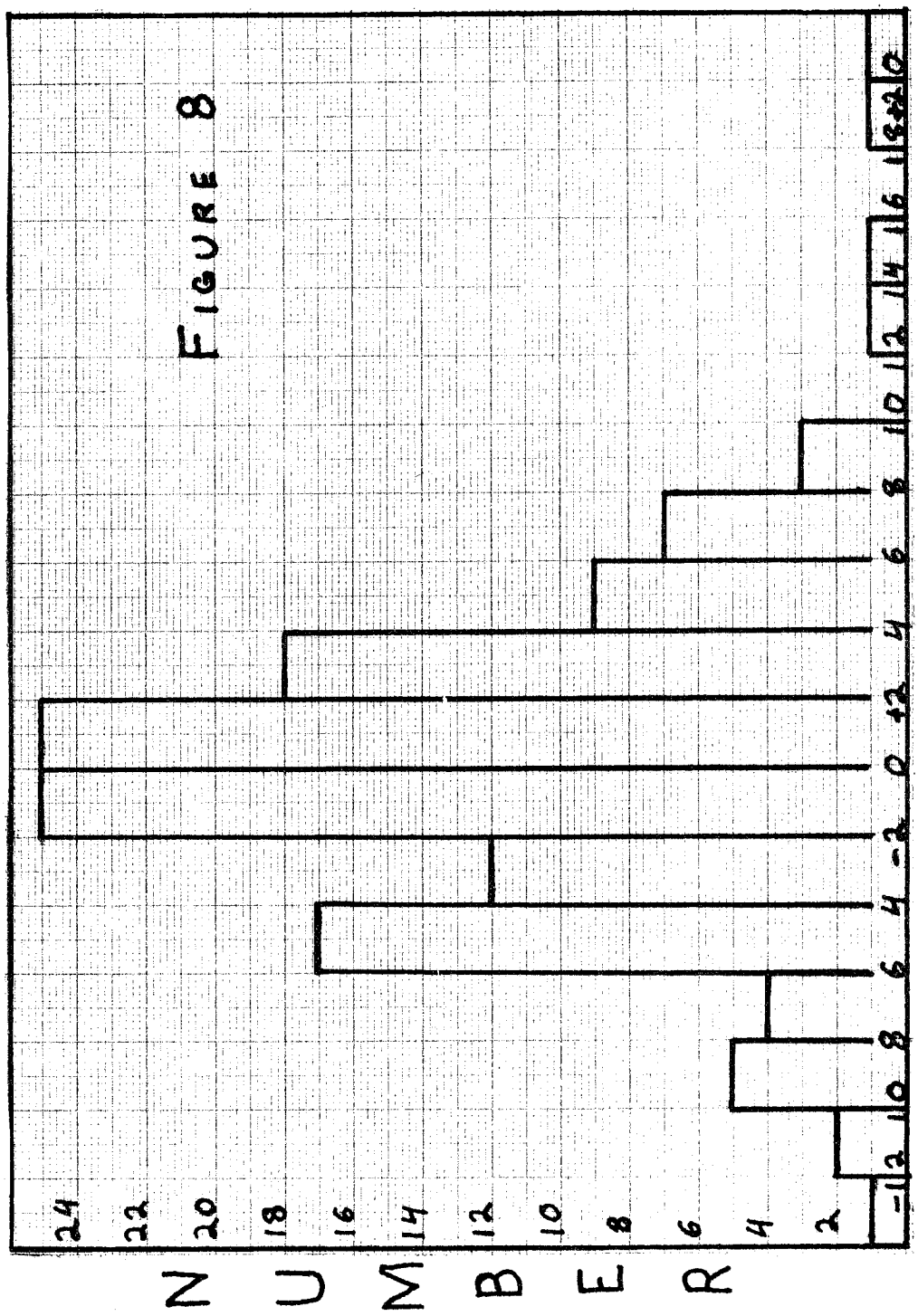
FIGURE 8
NUMBER
24
22
20
18
16
14
12
10
8
6
4
2
-12 -10 -8 -6 -4 -2 0 +2 4 6 8 10 12 14 16 18 +20
σα - degrees

FIGURE 9: Histogram of the standard deviations, σ_v, of those radial velocities from Table IV which were determined from more than one emission line.

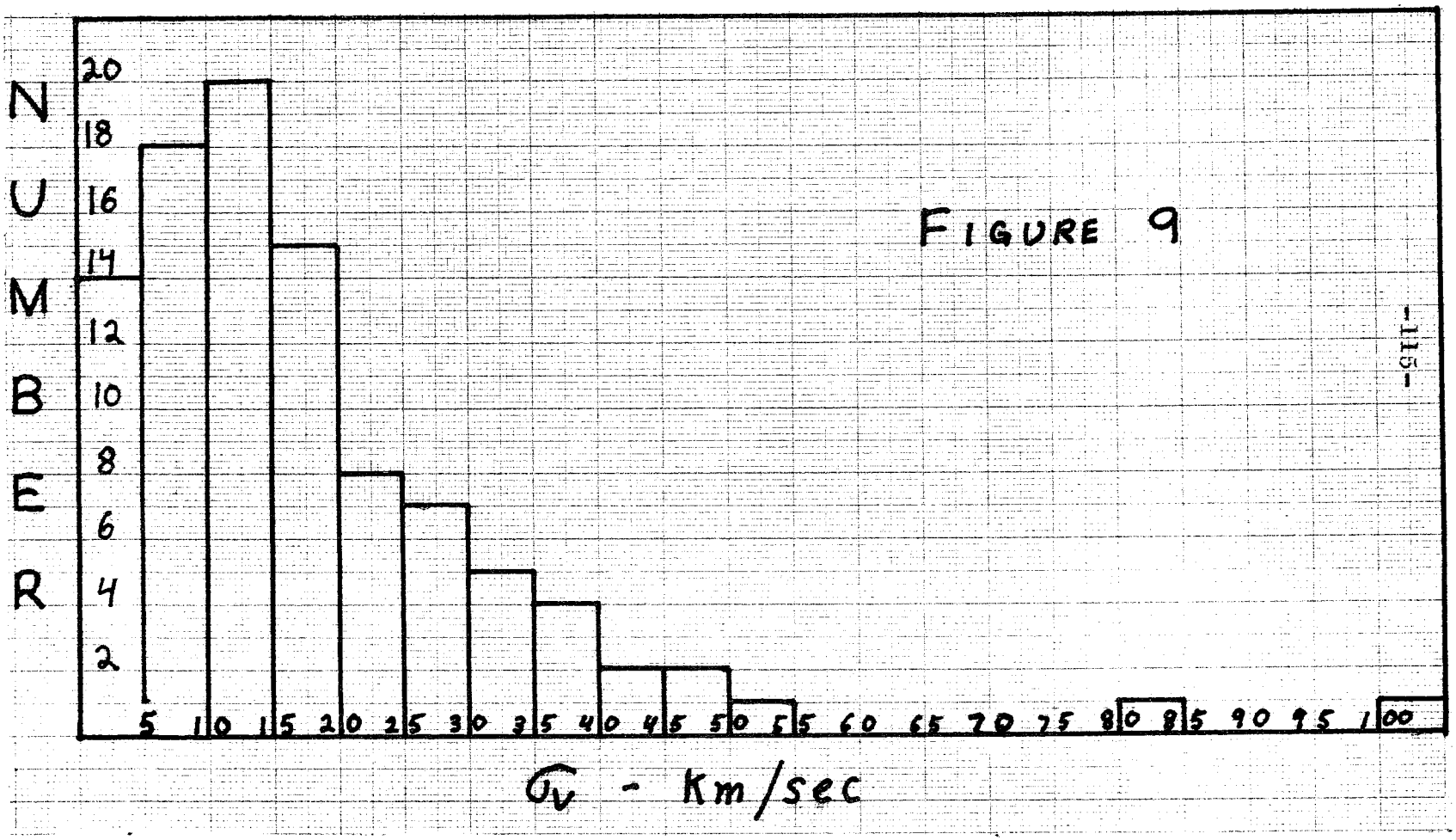
NUMBER
20
18
16
14
12
10
8
6
4
2
5 10 15 20 25 30 35 40 45 50 55 60 65 70 75 80 85 90 95 100
σ_v - Km/sec

FIGURE 9

FIGURE 10: Zero-epoch positions of the filaments measured only for proper motion as determined from 100 in. plates. The five stars near the center of the nebula and the directions of the major and minor axes are shown. The position of the expansion center is indicated by arrows near the edge of the figure.

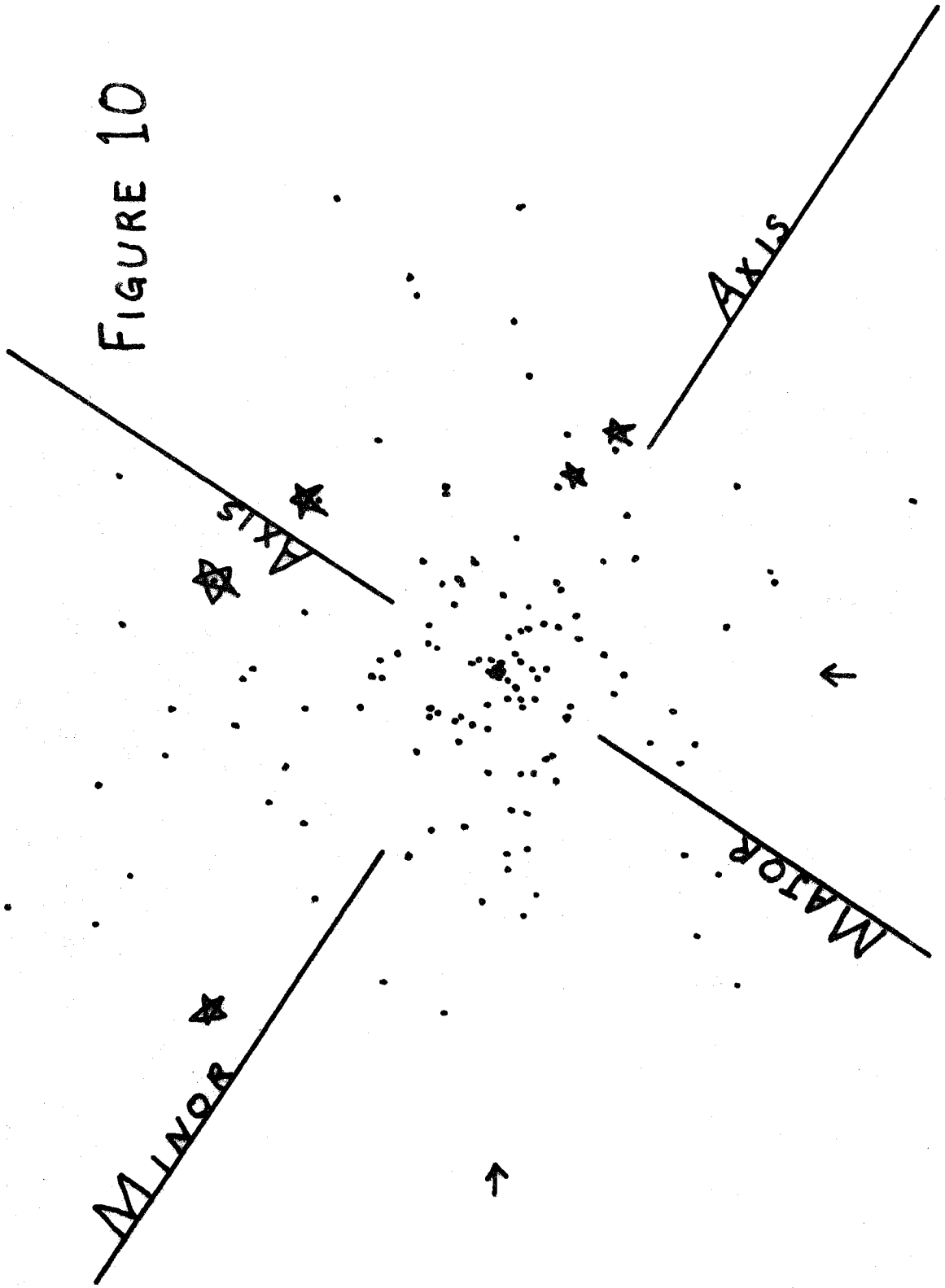

FIGURE 10

FIGURE 11: Zero-epoch positions of the filaments measured only for proper motion as determined from 200 in. plates. The central stars, major and minor axes, and the expansion center are shown as in Figure 10.

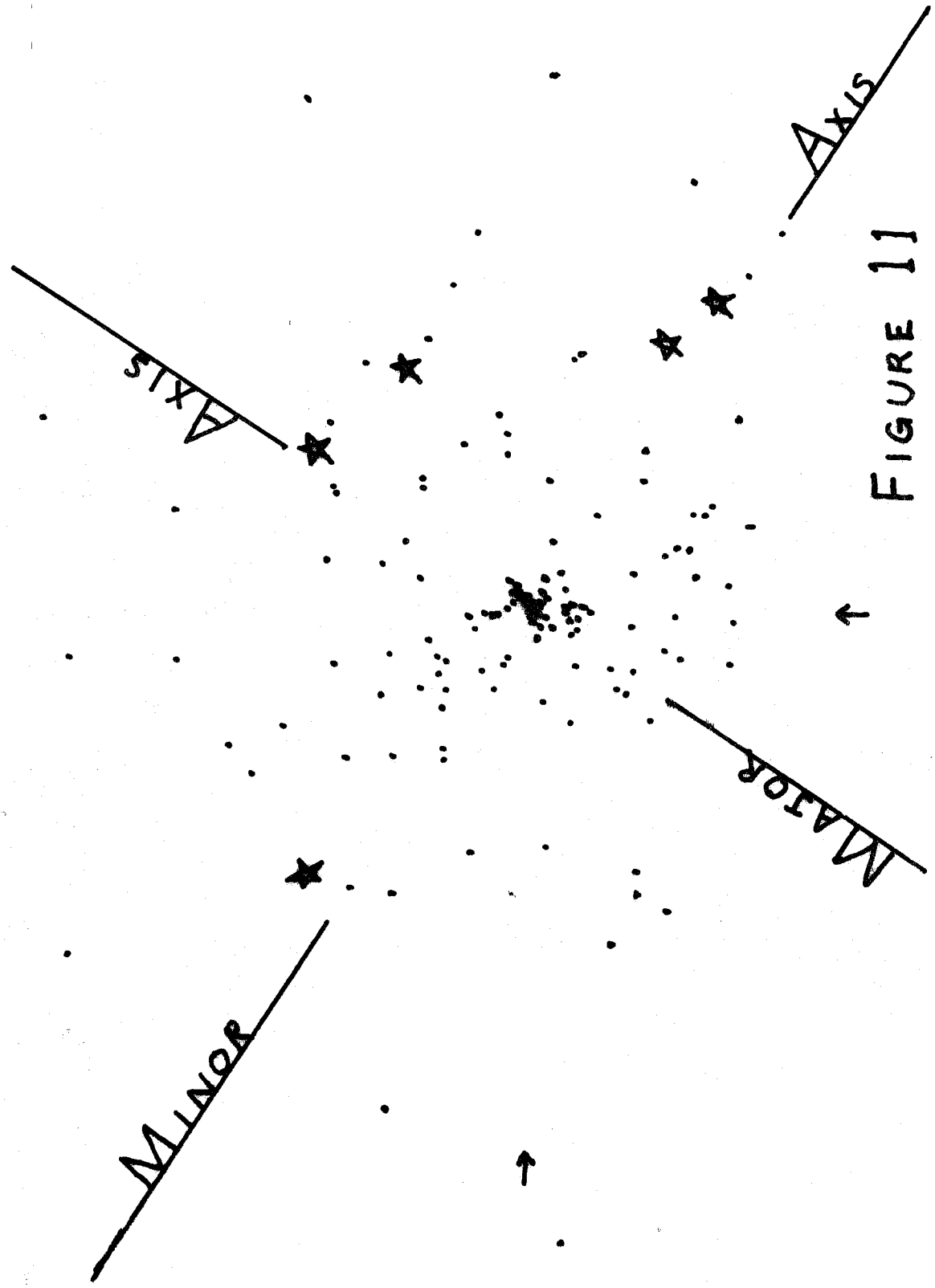

FIGURE 11

FIGURE 12: Histogram of the dates of closest approach to the expansion center by the filaments measured only for proper motion (shown in Figure 1 and Table III) as determined from 100 in. plates.

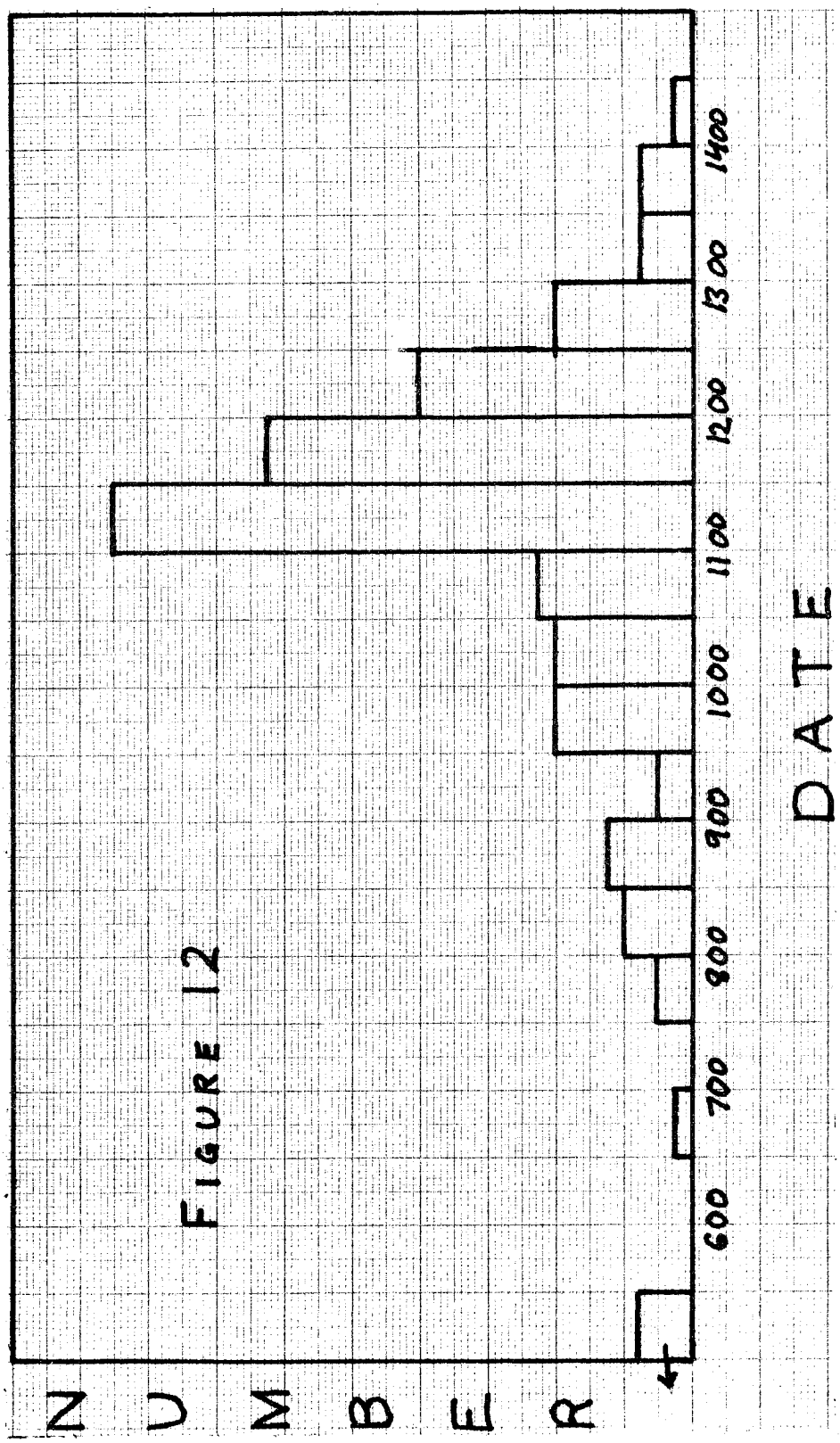

FIGURE 12

FIGURE 13: Histogram of the dates of closest approach to the expansion center by the filaments measured only for proper motion (shown in Figure 1 and Table III) as determined from 200 in. plates.

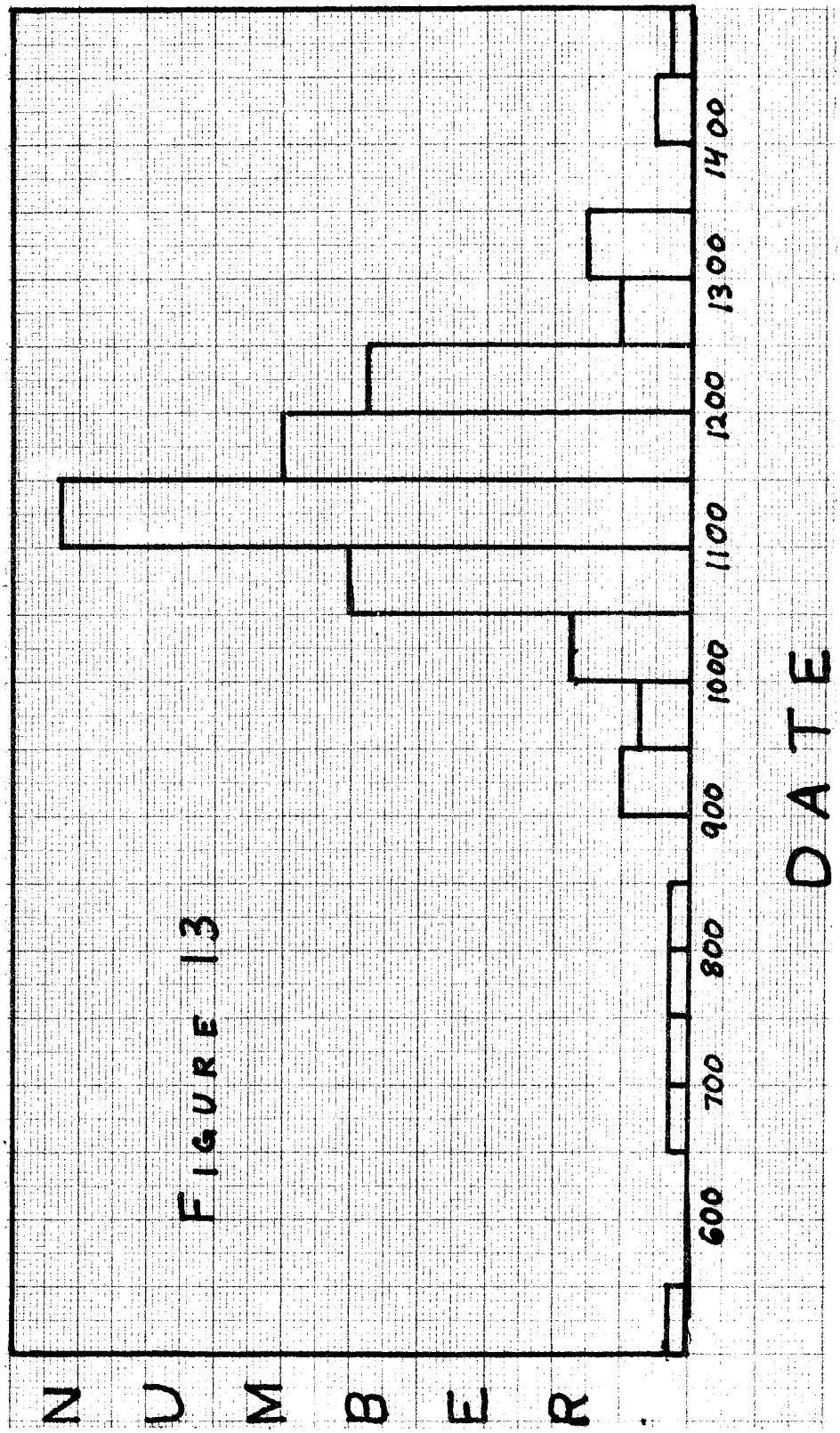

FIGURE 13

FIGURE 14: Histogram of the quantity $(r - \mu t)/r \times 100\%$ which measures deviations from the general rule that the length of the proper motion vector of a given filament is proportional to its distance from the center of the nebula.

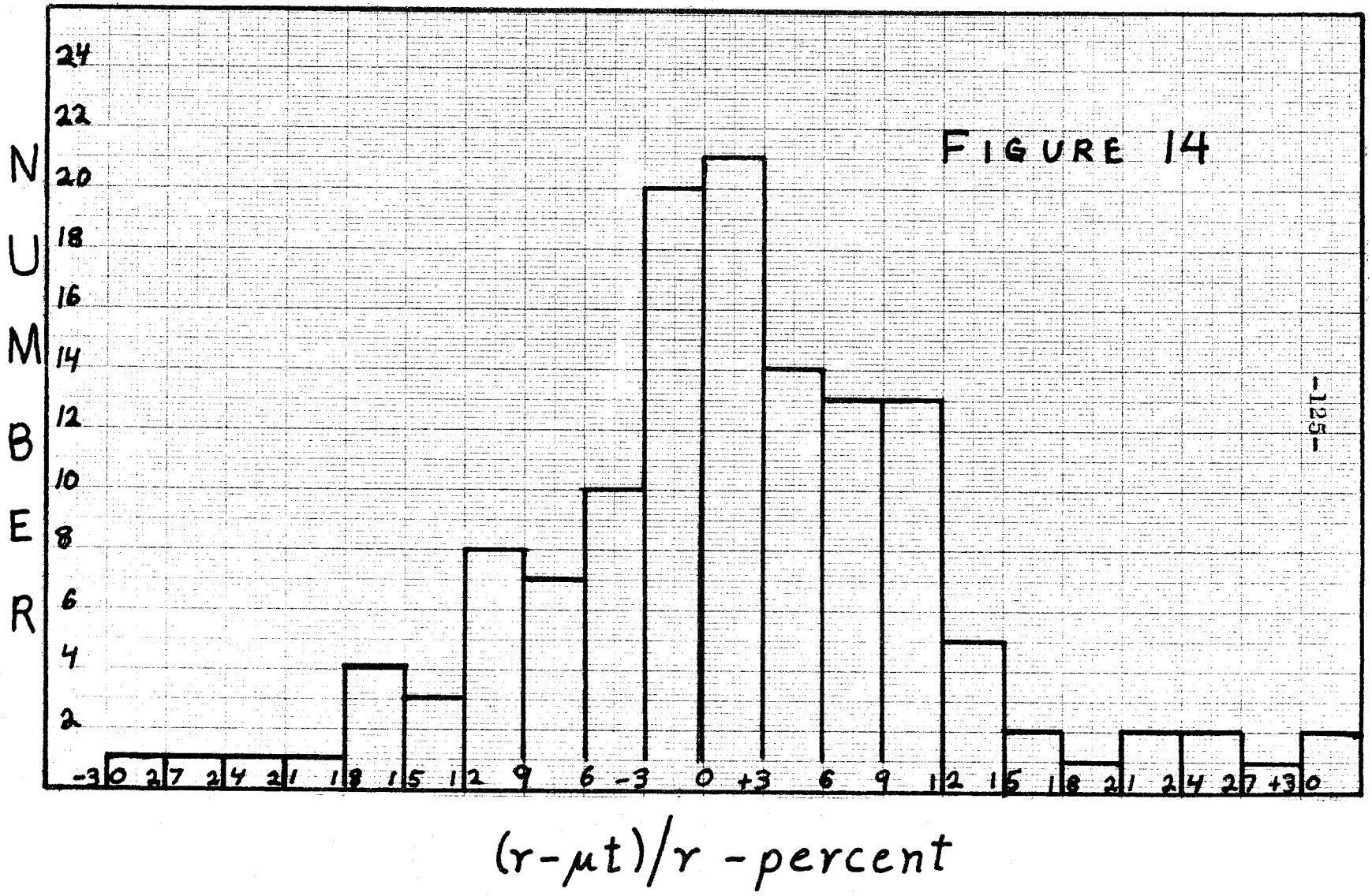
FIGURE 14
NUMBER
24
22
20
18
16
14
12
10
8
6
4
2
-3 0 2 7 2 4 2 1 1 8 1 5 1 2 9 6 -3 0 +3 6 9 1 2 1 5 1 8 2 1 2 4 2 7 +3 0
(r-μt)/r - percent

FIGURE 15: Histogram of the quantity $(\tan^{-1} y/x - \tan^{-1} \mu_y/\mu_x)$, which is the difference in position angle between the radius to the filament and its present direction of motion.

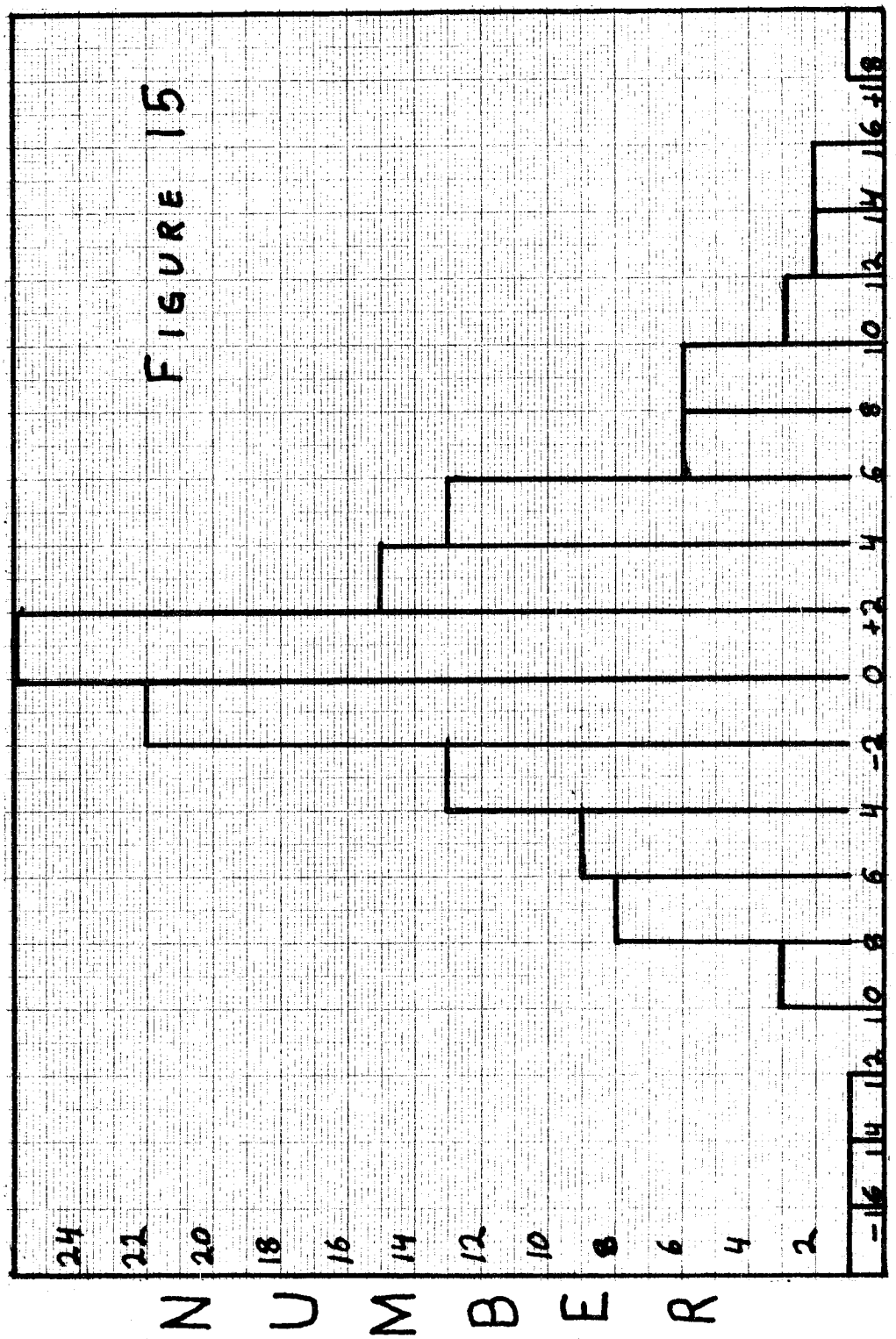
FIGURE 15
NUMBER
24
22
20
18
16
14
12
10
8
6
4
2
-16 -14 -12 -10 -8 -6 -4 -2 0 +2 4 6 8 10 12 14 16 +18
Tan⁻¹ (y/x) - Tan⁻¹ (μy/μx) - degrees

FIGURE 16: The electromagnetic radiation from the Crab Nebula. Sources of the various data points are given by Haymes et al. (1968). The shaded region represents the possible spectra in the optical if the absorption is between $1^m.1$ and $3^m.2$. The soft x-ray spectrum is shown as emitted if there is no absorption and for the absorption expected out to 1 and 2 kpc.

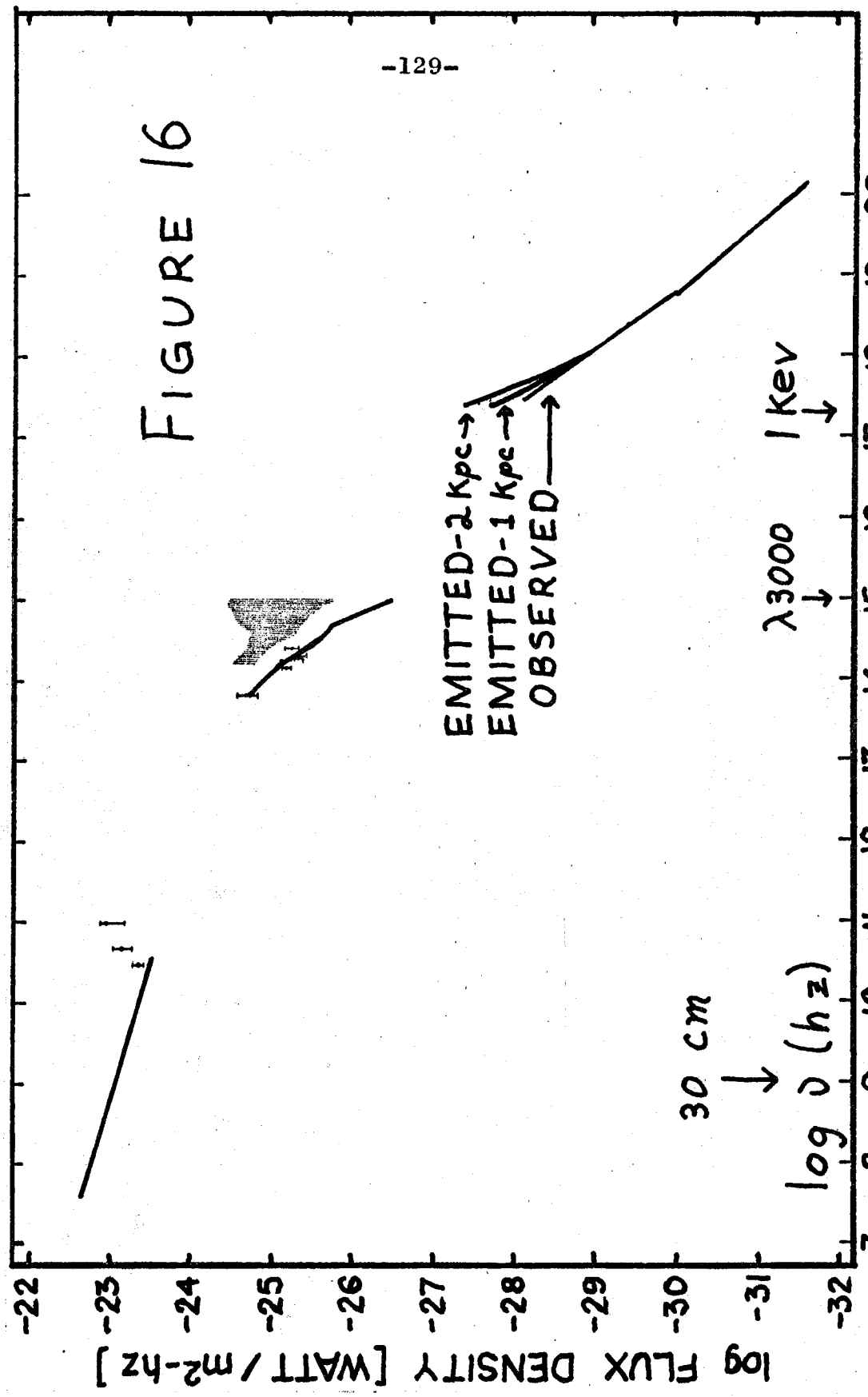
log FLUX DENSITY [WATT / m²-hz]
-22
-23
-24
-25
-26
-27
-28
-29
-30
-31
-32
log ν (hz)
7
8
9
10
11
12
13
14
15
16
17
18
19
20
30 cm
λ3000
1 Kev
EMITTED-2 Kpc→
EMITTED-1 Kpc→
OBSERVED→

FIGURE 16

FIGURE 17: Sketch of the Crab Nebula showing those regions and features discussed in section V.F.

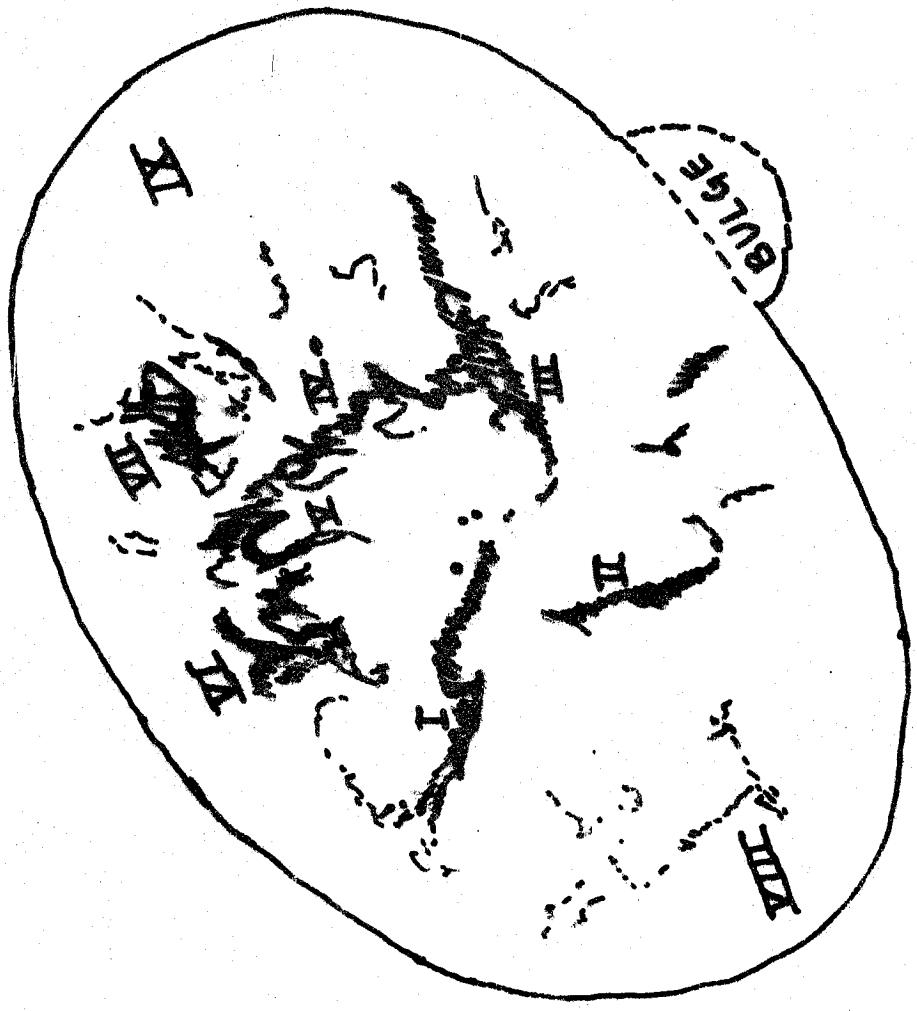

FIGURE 17